PAPER

Check for updates

Copper-modified graphene oxide and reduced graphene oxide nanocomposites for the photo-assisted removal of basic blue-3 dye

Ubaid Ur Rahman,[a] Abbas Khan, [ID][ab] Asadullah,[a] Muhammad Humayun,*[b] Nasrullah Shah,[a] Amal Faleh Alanazi [ID][b] and Mohamed Bououdina[b]

Basic Blue 3 (BB3) dye is a very contaminating substance that poses a substantial risk to human health and the environment. To solve this issue, we synthesized carbon-based materials, such as graphene oxide (GO), reduced graphene oxide (R-GO), and their nanocomposites, which demonstrated exceptional potential for the photo-assisted removal of BB3 dye. Pristine GO and R-GO were synthesized using a modified Hummers' method, while copper (Cu) nanoparticles (NPs) were incorporated through a simple co-precipitation method to boost the photocatalytic performance of the resultant hybrid materials. A detailed characterization of these synthesized nano-materials was performed using several analytical techniques to understand their structural, morphological, and chemical properties. Characterization results confirmed the successful fabrication of the desired hybrid nanocomposites. The photo-assisted removal of BB3 dye using synthesized nano-materials was evaluated under a batch methodology, changing the experimental conditions to optimize BB3 dye removal from wastewater. The results exhibited that Cu@R-GO and Cu@GO nanocomposites exhibited notable photocatalytic performance, accomplishing maximum removal rates of 75.41% and 68.05%, respectively. These values were meaningfully higher than those of R-GO (44.92%) and GO (35.11%) under the same experimental conditions. Furthermore, to increase insights into the degradation mechanism, the experimental data were analyzed using thermodynamic and kinetic models. The results indicate that the Cu@R-GO nanocomposite not only possesses excellent degradation abilities but also displays promising thermodynamic and kinetic parameters for the photo-assisted removal of BB3 dye. The results of our study clearly indicate that the Cu@R-GO nanocomposite as an outstanding candidate for the photocatalytic removal of impurities from wastewater, offering a possible solution for environmental remediation.

1 Introduction

Dyes are highly challenging contaminants generated by various industries, including textiles, cosmetics, rubber, plastic, paper, food, printing, and pharmaceuticals.[1] Due to the presence of hazardous and organic waste in wastewater and visible pollution in surface water, minimizing the amount of organic dyes and nitro compounds has become a fundamental and remarkably compelling problem.[2] Furthermore, the discharge of these colored compounds directly or indirectly into the ecosystem is very toxic to animals, plants, and human health.[3] Therefore, it is desirable to develop innovative methods capable of powerfully breaking down organic dyes and nitro compounds in wastewater into non-toxic molecules.[4] Meanwhile, their complex

structure, synthetic origin, high biological and chemical stability, and incomplete solubility in water, as well as converting azo dyes into harmless chemicals and nitro compounds into useful compounds, present challenges.[5]

The removal of dyes from wastewater can be achieved through various methods, such as physical, biological, and chemical processes.[6] However, each technique possesses distinct physical properties and varying levels of efficiency.[7] Due to its rapid reaction rate, the chemical approach is often considered a preferable method for dye removal.[8] Consequently, there is a critical need to develop advanced materials capable of degrading dyes and nitro compounds, which should exhibit high effectiveness, enhanced catalytic activity, robust physical–chemical and thermal stability, a large specific surface area, and efficient electron transfer capabilities.[9]

Additionally, carbon-based materials and their composites have attracted significant scientific attention due to their remarkable properties and potential applications in the energy and environmental sectors. Graphene, a two-dimensional

[a]Department of Chemistry, Abdul Wali Khan University, Mardan 23200, KP, Pakistan. E-mail: abbas053@gmail.com

[b]Energy, Water and Environment Lab, College of Humanities and Sciences, Prince Sultan University, Riyadh 11586, Saudi Arabia. E-mail: mhumayun@psu.edu.sa

monolayer of carbon atoms arranged in a hexagonal lattice, demonstrates an exceptional electronic structure and outstanding physicochemical properties. Owing to its distinctive structure and superior characteristics, researchers have been actively exploring its potential across diverse scientific fields.[10,11] Among the most notable carbon-based materials are graphene and its derivatives, graphene oxide (GO) and reduced graphene oxide (rGO). These materials exhibit unique attributes, including a high surface-to-volume ratio and cost-efficient synthesis. The integration of GO and rGO with semiconductor-based catalysts can significantly enhance photocatalytic performance.

Furthermore, the functionalization of graphene-based composites with specific groups and metal nanoparticles, such as copper,[12] zinc,[12] cobalt,[13] gold, silver,[14] and titanium oxide, can further optimize their properties.[15,16] Copper (Cu) serves as a practical modifier for graphene due to its affordability, optical properties, chemical stability, and non-toxic nature. Nano-copper finds applications in bandages,[17] biomaterials,[17] pharmaceuticals,[18] water purification systems,[19] and textile manufacturing.[20] Effective wastewater treatment and recycling are essential for ensuring water safety, particularly given the increasing global population and inadequate wastewater management, which are major contributors to water pollution.[21] Organic dyes, especially azo dyes containing the $-N{=}N-$ functional groups, are extensively used in industries, such as textiles, food, paper, paints, pharmaceuticals, cosmetics, and leather. These synthetic dyes, discharged in large quantities annually, impart significant color to wastewater and pose serious environmental challenges.[22,23] These synthetic dyes are extensively utilized in the production of diverse consumer and industrial goods, including textiles, leather, paper, paints, cosmetics, pharmaceuticals, and food products.[24] Basic Blue 3 (BB3), a cationic dye extensively utilized in the textile industry, poses significant health and environmental risks. Scientific and medical studies have linked BB3 exposure to skin irritation, lung cancer, allergic eye reactions, and skin inflammation.[25]

Therefore, for the removal of toxic materials from the ecosystem, different techniques have been used. Conventional techniques, such as coagulation, filtration, erosion, ultrafiltration, adsorption, and advanced oxidation processes (AOPs), have been employed to eliminate such toxic dyes from wastewater. However, these methods often prove costly and inefficient, sometimes exacerbating pollution issues.[26] In contrast, photocatalysis and adsorption have gained prominence due to their operational simplicity, high efficiency, ease of recovery, and adaptability.[27] These approaches also offer the advantage of catalyst reusability and the potential for complete mineralization of harmful degradation byproducts. Recent advancements have explored nanomaterial-based catalysts, including porous materials, activated carbon,[28] polymer-supported catalysts,[29] zeolites,[30] and metal oxides (*e.g.*, CuO, ZnO, and silica).[31] Of particular interest are metal-decorated graphene derivatives, such as TiO$_2$/GO, TiO$_2$/rGO, CuO–ZnO/GO, CuO–ZnO/rGO, Ag/rGO, Fe/rGO, and Pd/rGO, which exhibit superior degradation performance, synergistic effects, tunable properties, and multifunctional applicability.[32]

A recent study demonstrated the efficacy of hydrothermally synthesized GO, rGO, and Cu–rGO composites in adsorbing methylene blue (MB) at 40 mg L^{-1}, achieving removal efficiencies of 63%, 68%, and 94%, respectively.[33] Notably, metal-doped rGO composites have shown exceptional adsorption capabilities, with efficiencies reaching 91% for MB removal, underscoring their potential in wastewater treatment applications.[34] In addition, previously synthesized Cu/rGO-based materials have shown high adsorption efficiency for methylene blue and Congo red dyes, with percent removal of 92% and 93.16%, respectively.[35] However, based on existing literature, no studies have reported on Cu@GO and Cu@R-GO. Due to the extensive application of GO/rGO-based nanocomposites, it is important to enhance the overall properties of these materials. Therefore, this study focuses on improving GO and rGO by decorating them with copper nanoparticles.[36]

To date, research on the synthesis, characterization, and catalytic/photocatalytic applications of these hybrid nanomaterials has been relatively rare.[37] Our literature review reveals that only a limited number of studies have specifically examined the fabrication and environmental applications of copper-anchored graphene oxide Cu@GO and reduced graphene oxide Cu@R-GO nanocomposites. Despite these preliminary investigations, numerous critical aspects of these materials remain unexplored and require systematic examination.[38] The present work expansively reports this research gap by focusing on the controlled synthesis of Cu@GO and Cu@R-GO nanocomposites, their detailed structural and morphological characterization, and the assessment of their performance in photo-assisted environmental remediation applications. The synthesized nanocomposites were used for the elimination of Basic Blue 3 dye, which is a cationic triphenylmethane dye widely used in industrial applications, mostly in the textile industry. The removal mechanisms were thoroughly examined through combined thermodynamic and kinetic studies. The adsorption process was explored using pseudo-second-order kinetics, while temperature-dependent performance was evaluated through Arrhenius and Eyring equations. These methods allowed the determination of critical parameters, such as activation energy, Gibbs free energy change, enthalpy change, and entropy change. The composites displayed better catalytic performance as compared to pure R-GO and GO-based materials, accomplishing maximum BB3 dye (80 mg L^{-1}) removal efficiencies of 68.5% and 75.4% within 80 minutes. The thermodynamic and kinetic parameters were also estimated for the dye removal process. The study of thermodynamic and kinetic parameters of the synthesized Cu@GO and Cu@R-GO nanocomposites also offers valuable insight into their potential applications in catalytic, photocatalytic, and adsorption processes, contributing to future environmental remediation approaches.

2 Experimental section

2.1. Chemicals and apparatus

The chemicals and reagents used in this research work include graphite (99%), sodium nitrate (99.99%), sulfuric acid (95–97%), potassium permanganate (99%), hydrogen peroxide (35%), ascorbic acid (98%), copper(II) sulfate hexahydrate

(99.99%), hydrochloric acid (37%), sodium hydroxide (97%) and basic blue 3 (BB3) (96–98%) dye, all obtained from Thermo Fisher Scientific. High-purity distilled water was used in all experimental procedures. All chemical components, obtained from Thermo Fisher Scientific, were of analytical grade and used without further purification. The experimental setup in this study involved the following instruments: a digital balance, magnetic hot plate stirrer, calibrated pH meter, and drying oven. Additional analytical equipment comprised a refrigerated centrifuge (Eppendorf, Model 5804R), UV light system (35 W, 254 nm), and UV-vis spectrophotometer (PerkinElmer, Lambda 35). Material characterization was achieved using X-ray diffraction (XRD; Bruker D8 Advance), field-emission scanning electron microscopy (FE-SEM; JEOL JSM-7001F) coupled with energy-dispersive X-ray spectroscopy (EDX; JEOL), differential scanning calorimetry (DSC 9), and Fourier-transform infrared spectroscopy (FTIR; PerkinElmer 100 FT-IR, USA).

2.2. Synthesis of graphene oxide

In a representative experiment, graphite was used as a core material, and graphene oxide was prepared using a modified Hummers' approach.[39] A specific amount of graphite (3 g) and 4 g of sodium nitrate ($NaNO_3$) were mixed in a 500 mL beaker. After mixing, 127 mL of sulfuric acid (H_2SO_4) was added and stirred for 75 minutes at a temperature below 5 °C. After that, 15 g of potassium permanganate ($KMnO_4$) was slowly added to the mixture over 2 h. Following this, 230 mL of distilled water was added, raising the temperature of the mixture to 95 °C, and stirring was continued for 45 min. Then, 30 mL of hydrogen peroxide (H_2O_2, 35%) was added dropwise, and the mixture was stirred overnight, resulting in a yellowish-color solution. The resulting mixture was washed with a 0.2 M hydrochloric acid (HCl) solution to remove residual sulfate (SO_4^{2-}) and nitrate (NO_3^{1-}) ions. Moreover, the resulting material was washed several times with distilled water until the pH of the mixture reached neutral (pH 7). Finally, the brownish color solution was centrifuged for 15 minutes at 8000 rpm.

2.3. Reduction of graphene oxide to reduce graphene oxide

To prepare reduced graphene oxide (R-GO), an L-ascorbic acid (L-AA) reduction technique was used.[40] In a typical experiment, 3 g of graphene oxide (GO) was dispersed in 120 mL of distilled water through sonication for 25 min to form a suitable GO suspension and 8 g of ascorbic acid was dissolved in 200 mL of distilled water. The mixture was stirred well until all the white L-AA powder completely disappeared. Furthermore, the solution was directly added to the GO suspension. The pH of the medium was adjusted to ~10 by adding 50 mL of 1.0 M ammonia solution (NH_3) dropwise, enhancing the colloidal stability through electrostatic repulsion. The solution was stirred on a hot plate at 25 °C for 24 h; after that, the final product was washed with ethanol and distilled water until the pH was neutralized. Finally, the solution was centrifuged and dried in an oven at 50 °C for 3 h.

2.4. Synthesis of Cu@GO and Cu@R-GO

Copper-modified graphene oxide Cu@GO and reduced graphene oxide Cu@R-GO nanocomposites were synthesized through a dropwise deposition method.[41] For this purpose, the pre-synthesized GO and R-GO were used. As previously discussed in Section 2.3, R-GO was obtained by chemically reducing the pre-synthesized GO using L-ascorbic acid in aqueous solution at 25 °C for 24 h under constant stirring. This eco-friendly reduction procedure effectively removes oxygen-containing functional groups while preserving the structural integrity of the graphene backbone. The procedure involved the dispersion of 100 mL GO/RGO suspensions in 80 mL distilled water, followed by 25 min of sonication. Instantaneously, 0.883 g of copper(II) sulfate penta-hydrate was dissolved in 50 mL of distilled water and sonicated for 20 min. The GO suspension was then shifted to a magnetic stirrer, and the copper sulfate solution was introduced dropwise under continuous stirring. The reaction system was slowly heated to 80 °C and kept at this temperature for 3 h under constant agitation. The step may have induced partial reduction of GO in the Cu@GO sample. The pH was carefully adjusted to 12 through dropwise addition of 0.1 M NaOH solution, after which the mixture was stirred overnight. The resulting product was subjected to several washing cycles with distilled water to eliminate impurities and achieve neutral pH. Finally, the purification was attained through centrifugation at 8000 rpm for 8 min, followed by drying at 70 °C for 3 h, yielding the desired Cu@GO (light brown, indicating partial reduction), while Cu@R-GO nanocomposites (black powder) indicate full reduction.

2.5. Characterization of synthesized materials

The synthesized nano-materials underwent complete characterization to assess their structural, morphological, thermal, physicochemical, and textural properties. Four different samples, graphene oxide (GO), reduced graphene oxide (R-GO), copper-decorated graphene oxide (Cu@GO), and copper-decorated reduced graphene oxide (Cu@R-GO), were analyzed using various advanced characterization techniques. The analytical instrumentation included: ultraviolet-visible (UV-Vis) spectroscopy (PerkinElmer Lambda 35) for optical property analysis, scanning electron microscopy (SEM, JEOL JSM-7001F) coupled with energy-dispersive X-ray spectroscopy (EDX, JEOL) for morphological and elemental characterization, differential scanning calorimetry (DSC 9) for thermal behavior assessment, Fourier transform infrared spectroscopy (FTIR, PerkinElmer 100 FT-IR, USA) for functional group identification and X-ray diffraction (XRD, Bruker D8 Advance) with Cu Kα radiation ($\lambda = 1.5406$ Å) for crystallographic analysis. Additionally, X-ray photoelectron spectroscopy (XPS) was used to analyze the chemical states, while Raman spectroscopy was used for molecular fingerprinting and compound identification.

2.6. Assessment of the photocatalytic performance of the materials

The photocatalytic performance of GO, R-GO, Cu@GO, and Cu@R-GO was evaluated by investigating the photodegradation

behavior of Basic Blue 3 (BB3) dye at a concentration of 80 mg L^{-1}, with a light source Philips UV lamp 35 W at 254 nm. A UV-vis spectrometer, in the wavelength range 400 to 800 nm, was used for the analysis of photocatalysis data. In a typical experiment, a 100 mL BB3 dye solution was mixed with 100 mg of synthesized photocatalytic materials. To establish a consistent adsorption–desorption equilibrium without the corresponding degradation, the solution was first stirred in darkness for 25 min until a stable UV-vis absorbance at 654 nm confirmed the attainment of equilibrium. Subsequently, UV irradiation was commenced for photodegradation studies. The light-induced response was measured at desired time intervals, and the samples were collected periodically to analyze the photocatalytic degradation of BB3 using a UV-vis spectrometer at the maximum absorbance wavelength of 654 nm. To assess the photocatalytic performance of the materials, solutions of different concentrations (100 mg L^{-1}, 80 mg L^{-1}, 60 mg L^{-1} and 40 mg L^{-1}) were prepared from a 200 mg per L stock solution BB3. The synthesized nanomaterials, including GO, R-GO, Cu@GO, and Cu@R-GO, were used as catalysts for the degradation of BB3. Among them, Cu@R-GO showed the best performance under identical experimental conditions; hence, this material was selected for detailed studies. For the degradation study, 0.1 g of Cu@R-GO catalyst was dispersed in 100 mL of a BB3 dye solution (40 mg L^{-1}). The experiment was conducted under controlled parameters, such as pH ranging from 3–11, temperature (25–60 °C), and reaction time (30–80 min). The mixture was stirred continuously under UV-light treatment. After specific time intervals, samples were centrifuged (8000 rpm, 8 min) to remove the catalyst, and the dye sample was analyzed by UV-vis spectrophotometry (λ_{max} = 664 nm) to measure the remaining dye concentration. All assessments were performed in triplicate to ensure replicability, and control experiments were conducted by varying different parameters while keeping others constant. The removal efficiency and percentage degradation were calculated using the following equations.[42]

$$\% \text{ Degradation} = \frac{C_i - C_e}{C_i} \times 100 \qquad (1)$$

$$\text{Removal efficiency} = \frac{C_i - C_e}{m} \times V \qquad (2)$$

Here in eqn (1) and (2), C_i is the initial concentration of BB3 dye (mg L^{-1}), and C_e is the equilibrium concentration of BB3 dye after degradation at time t (mg L^{-1}). V represents the volume of the BB3 dye solution (L), and m represents the mass of the Cu@R-GO catalyst used (g).

2.6.1. Effect of experimental variable quantities on the photocatalytic degradation of basic blue 3. To investigate the impact of the experimental time on the photocatalytic degradation of BB3 dye using the synthesized catalysts, a fixed amount of dye concentration of 80 mg L^{-1} and 0.1 g of each catalyst (GO, R-GO, Cu@GO, and Cu@R-GO) were employed at different time intervals (0, 10, 20, 40, 60, 80, and 100 min). After each interval, the solution was centrifuged, and the remaining undegraded dye was determined using a UV-visible

spectrometer. To study the impact of initial dye concentration on photocatalytic efficiency, BB3 solutions of various concentrations (40, 60, 80 and 100 mg L^{-1}) were prepared and investigated while keeping other variables constant; reaction time = 80 min, temperature = 60 °C, pH = 7, UV-light source 35 W, and catalyst dose 0.1 g. The photocatalytic degradation performance was thoroughly assessed under controlled conditions to assess the temperature and pH effects. Temperature studies (40–80 °C) were conducted with fixed parameters: 80 min reaction time, 80 mg per L BB3 concentration, pH 7, 35 W UV irradiation, and 0.1 g catalyst dose. The corresponding pH experiments (pH 3–11) employed 0.1 M HCl/NaOH for pH tuning while keeping constant conditions: 80 min reaction time, 60 °C temperature, 0.1 g catalyst mass, and 80 mg L^{-1} dye concentration. This approach allowed for the isolated evaluation of the influence of each parameter on degradation efficiency. Additionally, the effect of hydrogen peroxide (H$_2$O$_2$) was investigated using different concentrations (1, 3, 5, 7 and 9 mM), while keeping constant experimental conditions; reaction time = 80 min, temperature = 60 °C, catalyst dose = 0.1 g, UV-light source 35 W, dye concentration = 80 mg L^{-1}, and pH = 7.

3 Results and discussion

3.1. Structural, morphological and chemical composition

3.1.1. X-ray diffraction (XRD). X-ray diffraction (XRD) was conducted to evaluate the phase composition and crystalline structure of the synthesized nanocomposites, as shown in Fig. 1. All samples, including GO, R-GO, Cu@GO, and Cu@R-GO, displayed diffraction patterns within the 2θ range of 5° to 80°. A distinct peak at 2$\theta \approx$ 11°, detected for GO, confirms the successful oxidation of graphite. This peak vanishes in both Cu@GO and Cu@R-GO samples, demonstrating the reduction of GO, mainly in Cu@R-GO, which was synthesized using L-ascorbic acid as a reducing agent. In the XRD pattern of Cu@GO, well defined peaks at 2θ values of 43.82°, 48.67°,
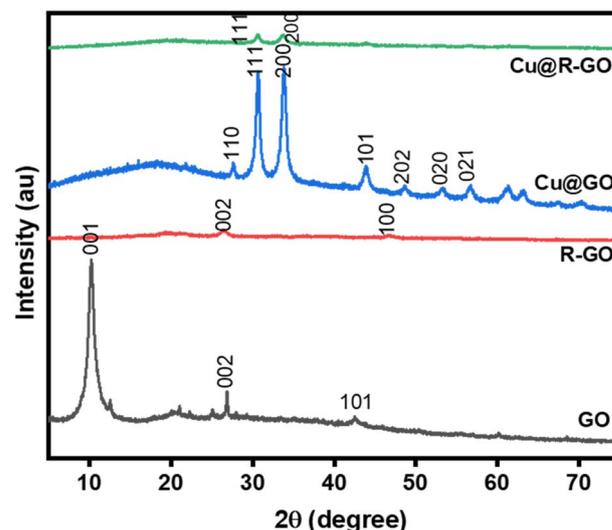

Fig. 1 XRD patterns of GO, R-GO, Cu@GO, and Cu@R-GO.

53.39°, 56.57°, and 61.15° resemble the (111), (200), and higher index planes of face-centered cubic metallic copper (Cu^0), (JCPDS 04-0836) confirming the effective reduction of $CuSO_4$ to elemental copper.[43] Additional peaks at 27.64°, 30.58°, and 33.88° corresponding to (110), (002), and (111) planes of Cu_2O are observed, suggesting the presence of minor oxidized copper species likely due to surface oxidation or exposure to air (JCPDS 05-0667).[44] In contrast, the Cu@R-GO sample displays broad peaks at 30.70° and 33.76°, characteristically associated with CuO and $Cu(OH)_2$, with no clear indication of metallic Cu, indicating the occurrence of oxidized copper species or very low copper crystallinity. Overall, the strong metallic copper signals in Cu@GO confirm successful reduction, while minor oxidized forms of Cu cannot be entirely exempted due to the surface sensitive nature of XRD and possible environmental exposure.

3.1.2. Scanning electron microscopy (SEM). Fig. 2 represents the scanning electron microscopy (SEM) analysis of the synthesized GO, R-GO, and their respective copper-based composites to examine their external surface morphology. As shown in Fig. 2 (a) GO, (b) R-GO, (c) Cu@GO, and (d) Cu@R-GO, the morphology and particle shape of GO appear asymmetrical. After the interaction of copper with GO, Fig. 2(c) shows that the copper is homogeneously dispersed on the surface of graphene oxide, with some cubic-like structure, which is also confirmed by XRD analysis. Following the reduction of graphene oxide to reduced graphene oxide, its morphology transformed into wrinkled sheets, as shown in Fig. 2(b). Fig. 2(d) shows the presence of a porous structure in the presence of tiny copper particles agglomerated on the surface of the materials. Furthermore, the presence of oxygen-containing functional groups, such as hydroxyl, carboxyl, and epoxide, within the inner layers may alter the surface characteristics of graphene oxide, making it rougher compared to R-GO.

3.1.3. Energy dispersive X-ray (EDX). Fig. 3 presents the elemental analysis of synthesized samples, including GO, R-GO, Cu@GO, and Cu@R-GO, investigated using energy-dispersive X-ray (EDX) spectroscopy. Fig. 3(a) corresponds to GO, (b) R-GO, (c) Cu@GO, and (d) Cu@R-GO nanocomposites. The primary peaks in Fig. 3(a) and (b) indicate the presence of carbon, oxygen, potassium, and trace impurities like sodium. In contrast, Fig. 3(c) and (d) reveal that the atomic weight percentages of carbon, oxygen and copper were 84.70%, 7.40%, and 7.90% for Cu@GO and 91.22%, 5.22%, and 3.55% for Cu@R-GO composites, respectively. These results confirm the successful fabrication of Cu@GO and Cu@R-GO composites. The experimental copper weight ratios, determined by EDX atomic percent analysis, were found to be 30.64 wt% for Cu@GO and 16.07 wt% for Cu@R-GO. These values deviate from the theoretical feed ratio, which was based on 0.883 g of copper(II) sulfate pentahydrate per 100 mg of GO/RGO (corresponding to 25.2 wt%). The discrepancy is likely due to the loss of unbound Cu^{2+} ions during the washing steps and the incomplete reduction of $CuSO_4$ in the aqueous phase. The reduced number of oxygen-containing functional groups in R-GO results in fewer available sites for Cu attachment compared to GO. Additionally, impurity peaks were observed in the samples (Fig. 3(a) and (b)), likely due to surface contaminants from the sample vessel during analysis, as well as trace impurities in the reagents used during synthesis. EDX analysis further confirmed a decrease in oxygen content and an increase in carbon content from GO to R-GO, indicating the successful chemical reduction of GO to R-GO.

3.1.4. X-ray photoelectron spectroscopy (XPS). To investigate the oxidation state of Cu and its interaction with GO and R-GO in the Cu@GO and Cu@R-GO nanocomposites, high-resolution X-ray photoelectron spectroscopy (XPS) was performed,[45] as depicted in Fig. 4(a and b). The Cu 2p spectra for
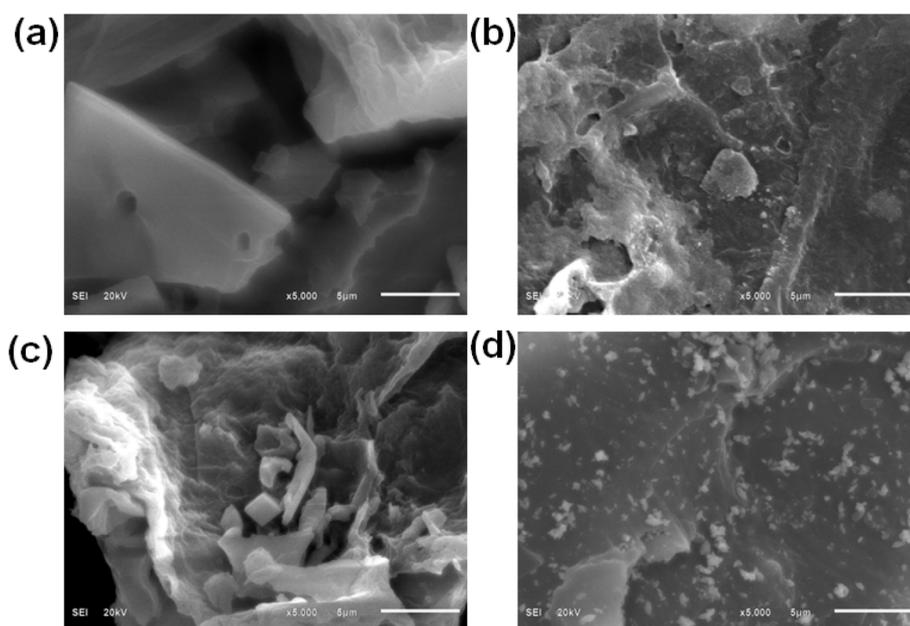

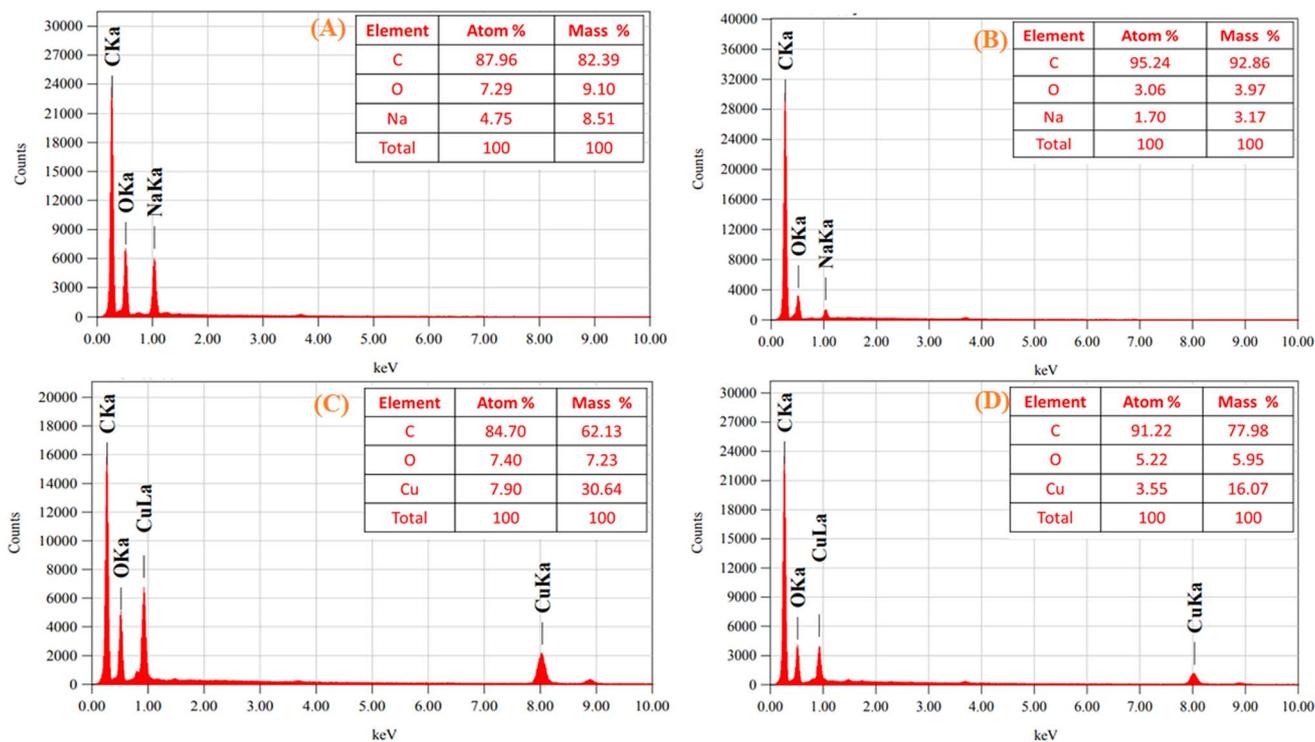Fig. 2 SEM images of (a) GO, (b) R-GO, (c) Cu@GO, and (d) Cu@R-GO.

Fig. 3 EDX analysis of (a) GO, (b) R-GO, (c) Cu@GO, and (d) Cu@R-GO nanocomposites.
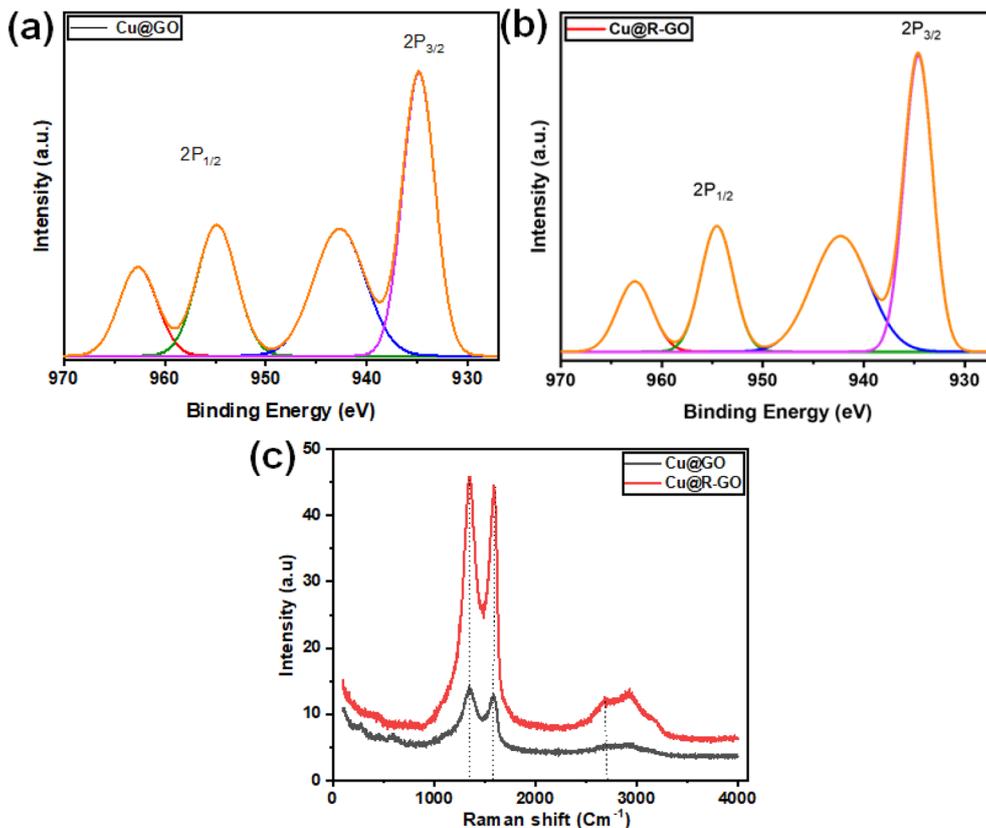

Fig. 4 XPS spectra (a and b) and Raman spectrum (c) of Cu@GO and Cu@R-GO nanocomposites.

both samples exhibit two prominent peaks located at approximately ~932.6 eV (Cu 2p$_{3/2}$) and ~952.4 eV (Cu 2p$_{1/2}$), which match the spin–orbit splitting of copper. These binding energies are characteristic of Cu^0 and Cu$^+$ species, confirming the presence of metallic copper and/or Cu(I) in the composites. In addition, weak satellite peaks were detected in the range of ~940–945 eV, suggesting a partial presence of Cu^{2+} species, indicative of a CuO-like environment. In the Cu@GO sample, Fig. 4(a), the Cu^{2+} satellite peaks are more pronounced, signifying a higher degree of copper oxidation. This is likely due to the abundance of oxygen-containing functional groups in GO, which tend to stabilize copper in its oxidized state. In contrast, the Cu@R-GO sample in Fig. 4(b) shows suggestively weaker Cu^{2+} satellite features, and the main Cu 2p$_{3/2}$ peak appears sharper and more intense. This indicates a greater proportion of Cu^0/Cu$^+$ species and suggests a stronger electron interaction with the π-conjugated network of R-GO. The observed reduction in the Cu^{2+} content in Cu@R-GO can be attributed to the partial exclusion of oxygen-based functional groups during the reduction of GO, which improves electronic communication and facilitates a more reducing environment. These results confirm the successful incorporation of copper into both GO and R-GO frameworks and highlight the different extents of metal–support interactions. Remarkably, R-GO provides a more conductive and reductive matrix, promoting better stabilization of lower-valence copper species.

3.1.5. Raman spectroscopy. Raman spectroscopy was performed to confirm the successful synthesis of Cu-based nanocomposites. As shown in Fig. 4(c), both samples (Cu@GO and Cu@R-GO) exhibited prominent D and G bands at about 1350 cm^{-1} and 1580 cm^{-1}, respectively.[46] The D band is related to structural defects and disordered sp^2 carbon, whereas the G band corresponds to the in-plane vibrations of sp^2 carbon atoms. The intensity ratio of I(D)/I(G) varied between the two samples. In Cu@GO, the higher ratio shows a higher degree of disorder, likely due to the presence of oxygen-containing functional groups. On the other hand, Cu@R-GO exhibited a lower I(D)/I(G) ratio, suggesting partial restoration of graphitic domains after reduction with ʟ-ascorbic acid. Moreover, the 2D band (~2700 cm^{-1}) appeared broader and weaker in Cu@GO, but became sharper in Cu@R-GO, further confirming enhanced structural ordering upon reduction. These results demonstrate that ʟ-ascorbic acid effectively reduced graphene oxide to reduced graphene oxide (R-GO), while the incorporation of Cu nanoparticles did not significantly disturb the graphene structure. The results are consistent with previous reports on the Raman peaks of reduced graphene oxide.

3.1.6. Thermo-gravimetric analysis and differential scanning calorimetry (TGA/DSC). TGA analysis of the synthesized particles was performed using a STD 600 TGA/DSC with a heating rate of 10 °C min^{-1} under airflow conditions at a rate of 60 mL min^{-1}. The results of TGA data, as shown in Fig. 5(a), illustrate the typical mass loss behavior concerning temperature, demonstrating the thermograms of carbonaceous species. For graphene oxide, the analysis of the curves indicates three significant weight loss stages within the temperature ranges of
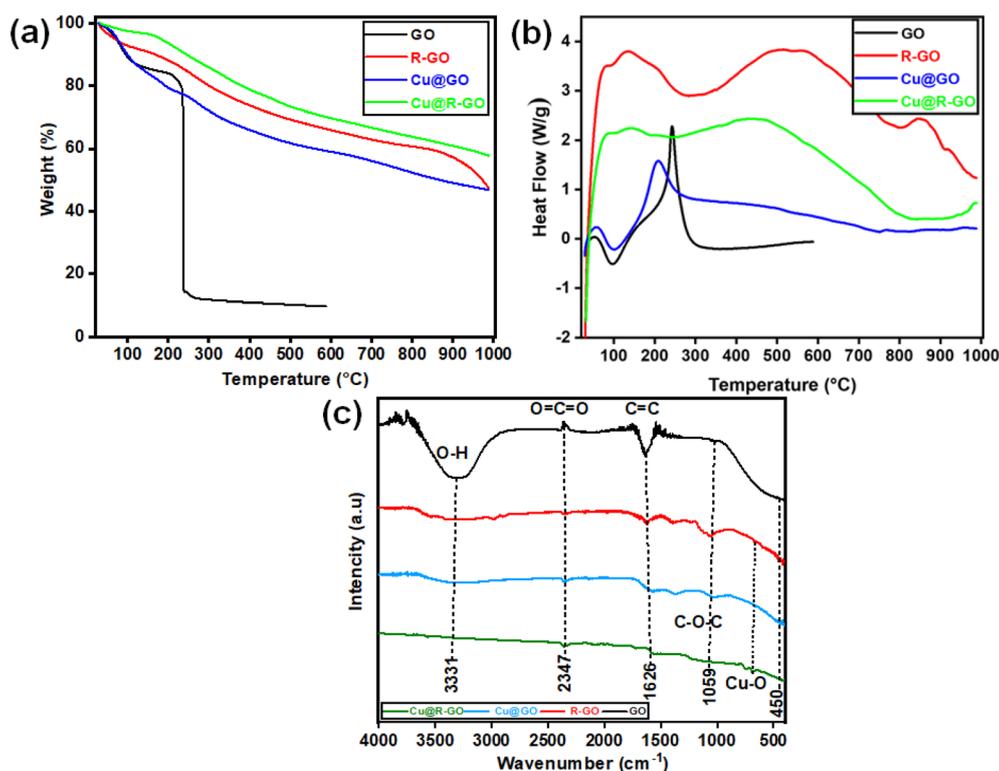

Fig. 5 Thermal and spectroscopic characterization of GO, R-GO, Cu@GO, and Cu@R-GO using (a) thermogravimetric analysis (TGA), (b) differential scanning calorimetry (DSC), and (c) Fourier transform infrared (FTIR) spectroscopy.

© 2025 The Author(s). Published by the Royal Society of Chemistry

33–130 °C and 130–270 °C.[47] The first weight loss (~3%) is attributed to the desorption of water molecules trapped on the surface of graphene oxides. The second and most significant weight loss of ~95% is mainly due to the decomposition of graphene layers containing labile oxygenated functional groups, which are converted into CO, CO_2, and steam. The third stage, occurring in the range from 280 °C to 457 °C, corresponds to the removal of more stable oxygenated groups, resulting in a minor weight loss of approximately 1.8%. The final and remaining amount of the sample (~0.8%) is attributed to potassium salts.

In the DSC analysis of graphene oxide and reduced graphene oxide, the first endothermic peak, observed at approximately 100 °C, relates to the loss of moisture from the powder, indicating energy absorption related to the evaporation of water. In contrast, the exothermic peak at around 290 °C is attributed to the thermal breakdown of the carbon skeleton. To reduce graphene oxide, an exothermic peak appears at almost 255 °C, which is lower than that of graphene oxide. This peak is related to the decomposition of hydroxyl and epoxy functional groups. During heating, the above-mentioned groups are eliminated, releasing energy and allowing R-GO to transition into a more thermally stable structure. The initial exothermic peaks in the DSC investigation of Cu@GO and Cu@R-GO are attributed to crystallization and chemical bonding processes taking place during heating. Furthermore, slight endothermic peaks observed in the range of 500–700 °C for both materials correspond to the conversion of amorphous copper (Cu) into its crystalline phase. This phase change includes energy

absorption, leading to the characteristic endothermic behavior, as shown in Fig. 5(b). The overall thermal analysis indicates that the synthesized materials exhibit thermal stability, making them suitable for potential applications at higher temperatures.

3.1.7. Fourier transform infrared spectroscopy (FT-IR). A comparative analysis of the FT-IR spectra of GO, R-GO, Cu@GO, and Cu@R-GO is shown in Fig. 5(c). The broad peak at 3331 cm^{-1} shows the stretching of the hydroxyl (OH) group, attributed to the vibration of water molecules. The transmittance peak at 2347 cm^{-1} points to the occurrence of CO_2, signifying its absorption from the atmosphere during synthesis.[34] The peak located at 1626 cm^{-1} denotes the aromatic C=C stretching, which is linked to the sp^2-hybridized nature of graphite, a characteristic that is also observed in the XRD analysis. The bands in the range of 1000–1300 cm^{-1} are attributed to C–O stretching vibrations and oxygenated functional groups. A decrease in their strength in the reduced and decorated samples proves the successful reduction of graphene oxide. In the FT-IR spectra of Cu@GO and Cu@R-GO, a new peak appears at 667 cm^{-1}, corresponding to the Cu–O bond. Additionally, the lower transmittance of vibrational and bending intensities of hydroxyl groups pointed toward the hydrophilic nature of reduced graphene oxide.

3.1.8. UV-visible and bandgap study of Cu@GO and Cu@R-GO. The UV-visible spectra of the samples are shown in Fig. 6(a–d). As expected, GO, R-GO, Cu@GO, and Cu@R-GO exhibit absorbance in the ranges of 230–280 nm, 240–300 nm, 240–600 nm, and 240–600 nm, respectively. In Cu@GO and Cu@R-GO, a smaller peak observed between 430–500 nm is
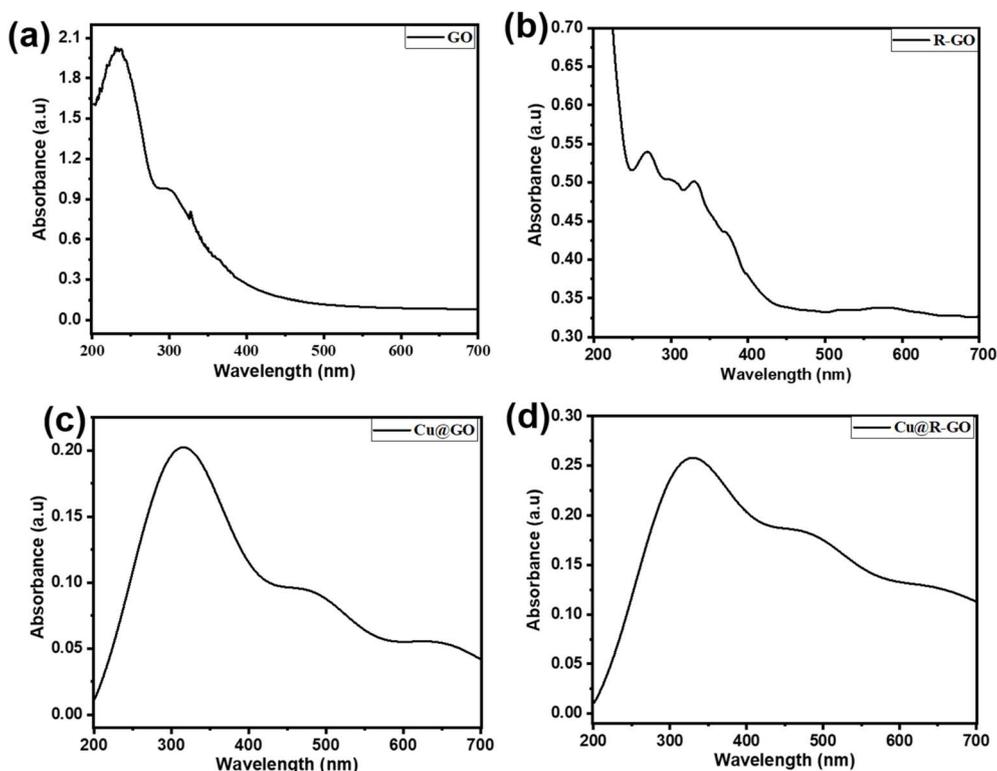

Fig. 6 UV-visible spectra of (a) GO, (b) R-GO, (c) Cu@GO, and (d) Cu@R-GO.

attributed to the presence of Cu, with its low intensity indicating a low Cu amount in the composite. The band-gap energies of GO, R-GO, Cu@GO, and Cu@R-GO were calculated using the Tauc plot equation, as presented in SI (Fig. S1(a–d)).

$$(\alpha h\nu)\gamma = A(h\nu - E_g) \quad (3)$$

In the Tauc plot equation, the variables are defined as follows: α denotes the absorption coefficient, h is the Planck's constant, ν represents photon frequency, A is a proportionality constant, E_g indicates the bandgap energy, and γ characterizes the electronic transition nature, implementing values of 1/2, 1/3, 2, or 2/3 depending on the specific transition type. The bandgap energy was determined by constructing a plot of $(\alpha h\nu)^{1/2}$ (in units of $(eV\ cm^{-1})^{1/2}$) against photon energy (eV). The linear region of this plot was extrapolated to the energy axis (X-axis) intercept to obtain the bandgap values. Through this analysis, the calculated bandgap energies were determined to be 2.81 eV for GO, 2.66 eV for RGO, 2.18 eV for Cu@GO, and 2.05 eV for Cu@R-GO, demonstrating a progressive decrease in bandgap energy with successive material modifications. This improvement can be attributed to the synergistic effect of Cu nanoparticles, which encourage electron transfer and reduce charge recombination in the reduced graphene oxide matrix. Especially, the bandgap values gradually decrease from GO to R-GO and then Cu@R-GO. Earlier studies have reported bandgap values for GO (4.09 eV),[48] R-GO (2.21 eV),[49] Cu-GO (1.06 eV),[50] and CuO-rGO (1.4 eV).[51] The observed differences in bandgap values confirm the successful fabrication of the nanomaterials and further support their

potential application as photocatalysts. The variation in bandgap values both among GO, R-GO, Cu@GO, and Cu@R-GO, as well as compared to the previous reports, may be due to some factors, such as structural variations, environmental aspects, decoration or doping, and the degree of reduction, synthesis approaches, experimental conditions, and the overall chemical composition of the synthesized nanomaterials. The declining bandgap values specify improved light absorption capacity and propose better photocatalytic potential of modified nanocomposites.

3.2. Photo-assisted removal of BB3 dye

The experimental details are given in Section 2.6. A typical experiment was initially conducted for 25 min in the absence of light to establish the adsorption–desorption equilibrium between the dye and the catalysts. Furthermore, a controlled experiment was also performed at the optimal time without using a catalyst (photolysis). In the absence of a catalyst, the degradation of the dye was negligible. Following this, the reaction mixture was exposed to UV light, and the catalyst was also used to achieve better outcomes.

3.2.1. UV-visible spectra of BB3 dye. The time-dependent UV-visible spectral changes of BB3 dye under photo-assisted removal using different catalysts, such as graphene oxide (GO), reduced graphene oxide (R-GO), copper decorated graphene oxide (Cu@GO) and copper decorated reduced graphene oxide (Cu@R-GO), are shown in SI (Fig. S2(a–d)). The degradation process was evaluated by detecting the reduction in the
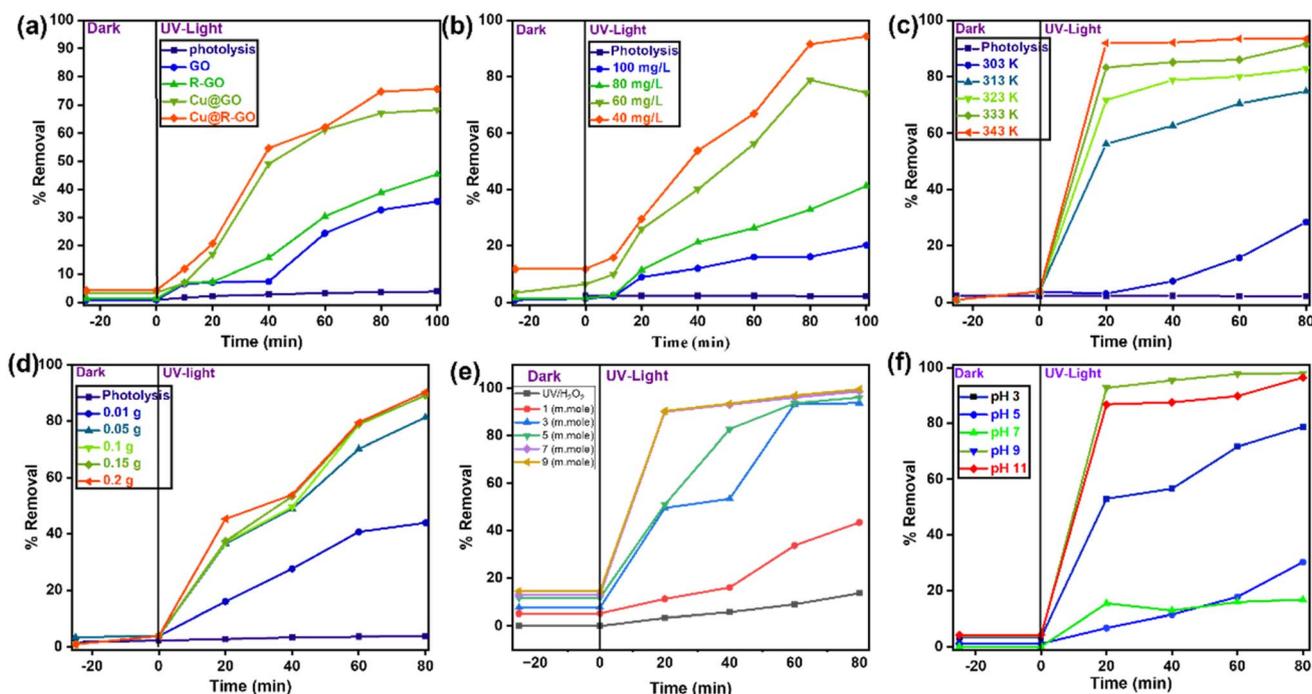

Fig. 7 Photo-assisted removal of BB3 (a) effect of time in the presence of GO, rGO, Cu@GO and Cu@R-GO, (b) effect of dye (BB3) concentration, (c) effect of temperature, (d) effect of catalyst amount, (e) effect of hydrogen peroxide (H_2O_2) and (f) effect of solution pH were investigated for some time in dark and under light without catalyst at different time intervals and changing all others parameters in each experiment.

absorption peak intensity within the visible range. The typical absorption band at 654 nm gradually reduced over time and eventually disappeared, confirming the complete breakdown of the dye molecules.

3.2.2. Effect of time on BB3 dye degradation. The photocatalytic performance of all synthesized materials (GO, RGO, Cu@GO, and Cu@R-GO) was scientifically evaluated for Basic Blue 3 (BB3) dye degradation under controlled conditions. Time-dependent studies were conducted at 20 min intervals over 25–100 min, while keeping constant experimental parameters (catalyst dose: 0.05 g L^{-1} in 100 mL solution; initial dye concentration: 80 mg L^{-1}). As shown in Fig. 7(a), the system reached equilibrium at 80 min, with the most noteworthy degradation occurring during the initial 10–80 min period, followed by saturation. Notably, Cu@R-GO demonstrated superior photocatalytic activity, achieving 75.40% dye removal at the equilibrium point (80 min), representing the highest degradation efficiency among all tested catalysts. Beyond this time-point, the equilibrium conditions are established, and the degradation process is significantly slowed; it is likely due to some possible reasons, such as recombination of electron–hole pairs, adsorption site saturation, and/or reduction in the reactive organic species (ROS).[52] It was observed that the degradation of BB3 during 60–80 min using Cu@GO and Cu@R-GO catalysts reached 68.05% and 75.40%, respectively. Since no appreciable increase in the percentage degradation and removal efficiency was observed beyond 80 min, this was considered an optimal time for further experiments. Furthermore, during the same time period, BB3 degradation using GO and R-GO catalysts was recorded at 35.12% and 44.91%, respectively. Based on these outcomes, it is evident that Cu@GO and Cu@R-GO catalysts show the best removal efficiencies towards BB3 dye. Therefore, further experiments were based on the Cu-decorated catalysts, maintaining the experimental time at 80 min while varying all other parameters, such as catalyst dose, temperature, pH, dye concentration, and H_2O_2 concentration.

3.2.3. Effect of initial BB3 concentration on its degradation. The photocatalytic degradation of Basic Blue 3 (BB3) dye was examined over a concentration range of 40 mg L^{-1} to 100 mg L^{-1}, while keeping all other experimental parameters constant. From these experiments, it was observed that an increase in the dye concentration led to a decrease in the photocatalytic efficiencies of the catalyst toward BB3 degradation. The maximum degradation (93.35%) was noted at a dye concentration of 40 mg L^{-1} of the dye, as shown in Fig. 7(b), while the minimum degradation occurred at 100 mg L^{-1} of BB3. This decline in the degradation efficiency at higher concentrations can possibly be attributed to an increased adsorption of more organic matter at the catalyst surface, which reduces the number of active sites on the surface of the catalyst. Therefore, the generation of hydroxyl radical (OH·) is reduced, leading to a decrease in the degradation efficiency.[53] In other words, at higher concentrations of BB3 dye, photons are refracted before reaching the surface of the catalyst; thus, the photocatalytic activity of the catalyst is decreased.[54] Based on these findings,

an optimal dye concentration of 80 mg L^{-1} was selected for further studies.

3.2.4. Effect of temperature on the degradation of BB3 dye. Photocatalytic efficiency of Cu@R-GO in the removal of BB3 dye was also evaluated at different temperatures ranging from 303 K to 343 K, while keeping other experimental parameters constant: reaction time = 80 min, pH = 7, catalyst concentration = 0.05 g L^{-1}, dye concentration = 80 mg L^{-1}, and UV-light source = 35 watt intensity. As illustrated in Fig. 7(c), an increase in temperature resulted in a higher rate of BB3 dye removal. Specifically, at 303 K, only 28% dye was removed in 80 min, whereas at 343 K, the removal efficiency increased to 93%. This reflects that this reaction is endothermic in nature. Furthermore, the temperature dependence of dye degradation is consistent with the earlier studies and aligns with Arrhenius theory, which states that the reaction rate is dependent on the temperature of the system.[55]

3.2.5. Effect of catalyst dosage. Fig. 7(d) demonstrated the effect of varying Cu@R-GO concentrations on the degradation of BB3 while keeping all the other experimental conditions constant. Catalyst dosage plays an important role in the dye-degradation process. It was observed that the degradation of dye increased by increasing the catalyst dose from 0.01 g L^{-1} to 0.2 g L^{-1}. However, a minimal increase was observed in dye degradation beyond the catalyst concentration of 0.1 g L^{-1}. This suggests that up to 0.1 g L^{-1}, the number of available active sites and the probability of interaction between the catalyst and dye molecules increase, enhancing the degradation process. Moreover, the generation of free electrons is responsible for the production of hydroxyl and superoxide radicals, which facilitate the degradation process.[56] The highest degradation efficiency, approximately 90%, was attained at the catalyst concentration of 0.1 g L^{-1}. Nevertheless, at a concentration beyond 0.1 g L^{-1}, nanoparticle agglomeration reduces the surface area and active sites, resulting in a decline in the dye degradation efficacy.[45]

3.2.6. Effect of hydrogen peroxide concentration on BB3 degradation. The effect of hydrogen peroxide (H_2O_2) on BB3 dye removal was studied using the same procedure as mentioned above, with the only variation being the concentration of H_2O_2, which ranged from 1 to 9 mM. All other parameters were kept constant: time (80 min), temperature (40 °C), pH (9), catalyst concentration (0.05 g L^{-1}), dye concentration (80 mg L^{-1}), and UV-light source (UV 35 watt intensity). H_2O_2 is a strong electron acceptor compared to oxygen due to its high oxidation potential and electrophilicity (ability to accept electron pairs).[57] Similarly, under identical experimental conditions, photolysis was performed using 9 mmol L^{-1} of H_2O_2. Results show that 13.36% elimination of BB3 after 80 min of UV exposure. It determines that only H_2O_2 alone acts as a mild oxidizing agent in the degradation process; however, the presence of a catalyst is essential to significantly enhance the degradation efficiency. The addition of H_2O_2 led to the enhanced generation of hydroxyl radicals and suppression of electron–hole pair recombination, thereby improving the photocatalytic degradation of BB3 dye, as confirmed by Fig. 7(e). The maximum degradation of BB3 (99.53%) was achieved at an H_2O_2 concentration of 9 mM using the Cu@R-GO catalyst.

3.2.7. Effect of pH of the medium on photocatalysis. The pH of the reaction medium plays a critical role in photocatalytic degradation processes, significantly influencing both hydroxyl radical generation and catalyst surface charge properties. Since industrial wastewater containing dyes is typically discharged across a wide pH range, we systematically evaluated Basic Blue 3 (BB3) degradation under varying pH conditions (3–11). The pH was precisely adjusted using 0.1 M HCl (for acidic conditions) and 0.1 M NaOH (for basic conditions), while maintaining all other experimental parameters constant. As demonstrated in Fig. 7(f), the degradation efficiency showed moderate enhancement from neutral to acidic pH, with optimal performance observed at pH 11. These findings clearly establish that solution pH directly modulates the surface charge characteristics of the catalyst and consequently affects its photocatalytic activity.[58] Moreover, pH also controls the ionization behavior of the dye, which influences the interaction between the dye molecules and the surface of the catalyst. These changes in pH can significantly affect the photocatalytic degradation process.

3.3. Expected photocatalytic mechanism for the removal of BB3 over Cu@R-GO
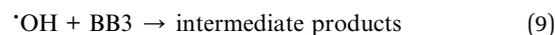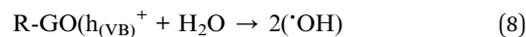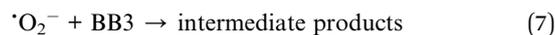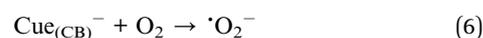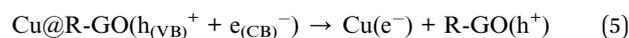
To justify the fundamental mechanism and control the leading reactive oxygen species (ROS) involved in BB3 dye degradation under optimal experimental conditions using Cu@R-GO, a series of scavenger experiments were performed (see SI, Fig. S3). Definite scavengers were introduced into the reaction system to selectively quench different ROS: isopropyl alcohol (IPA) was used to prevent hydroxyl radicals ($^\bullet$OH), benzoquinone (BQ) for superoxide radicals ($^\bullet$O$_2^-$), and (ethylenediaminetetraacetic acid disodium salt) EDTA-2Na for photogenerated holes (h$^+$). On the addition of IPA, the degradation proficiency abruptly decreased from 75.5% to 40.9%, demonstrating that $^\bullet$OH radicals are the primary reactive species carrying out the photocatalytic process. A moderate reduction to 48.6% in the presence of BQ indicates that superoxide radicals also play a notable role. When EDTA-2Na was introduced, a degradation rate of 60.2% was observed, pointing to a secondary yet substantial involvement of photogenerated holes. These results collectively confirm that all three species $^\bullet$OH, $^\bullet$O$_2^-$, and h$^+$ contribute to BB3 degradation, with hydroxyl radicals playing the principal role in the Cu@R-GO photocatalytic system.

Scheme 1 demonstrates the proposed photocatalytic degradation mechanism of Basic Blue 3 (BB3) dye using Cu@R-GO nanocomposites. Upon irradiation with light energy exceeding the bandgap of RGO, electron–hole pairs are generated through photoexcitation, where electrons (e$^-$) are promoted from the valence band (VB) to the conduction band (CB).[59] The inherent electric field at the Cu@R-GO interface facilitates efficient charge separation, significantly suppressing electron–hole recombination. Due to the Schottky barrier formation at the metal–semiconductor junction, photoexcited electrons migrate from the conduction band of R-GO to copper nanoparticles, driven by the work function difference between Cu (lower work function) and R-GO. This charge separation results in electron accumulation on Cu nanoparticles while holes remain localized
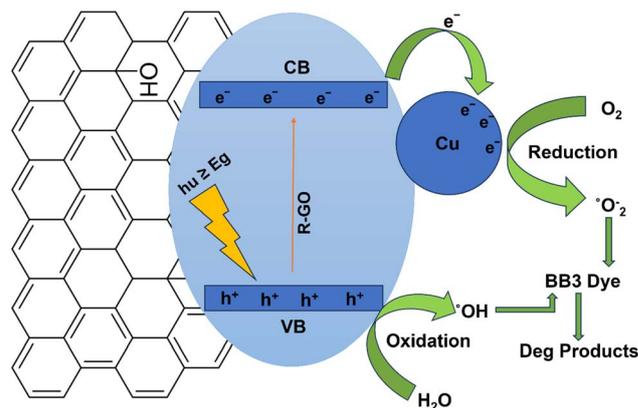
Scheme 1 Proposed mechanism for the photoassisted degradation of the BB3 dye over the Cu@R-GO.

in the R-GO matrix. The transferred electrons subsequently react with the adsorbed oxygen molecules to generate reactive oxygen species (ROS), particularly superoxide radicals ($^\bullet$O$_2^-$), which participate in the oxidative degradation of the adsorbed BB3 dye molecules. Simultaneously, the photogenerated holes in the R-GO valence band contribute to the direct oxidation of organic pollutants or react with surface hydroxyl groups to produce additional oxidizing species. These ROS then break down BB3 into intermediate molecules, ultimately decomposing it into CO$_2$ and H$_2$O. Meanwhile, the holes in R-GO participate in the oxidation of adsorbed water (H$_2$O), generating hydroxyl radicals ($^\bullet$OH), which further break down BB3 into intermediate molecules, CO$_2$, and H$_2$O. The important and fundamental reactions involved in the photo-assisted removal of BB3 over Cu@R-GO are outlined below.

$$Cu@R\text{-}GO + h\nu \rightarrow Cu@R\text{-}GO(h_{(VB)}^+ + e_{(CB)}^-) \quad (4)$$

$$Cu@R\text{-}GO(h_{(VB)}^+ + e_{(CB)}^-) \rightarrow Cu(e^-) + R\text{-}GO(h^+) \quad (5)$$

$$Cue_{(CB)}^- + O_2 \rightarrow {}^\bullet O_2^- \quad (6)$$

$${}^\bullet O_2^- + BB3 \rightarrow \text{intermediate products} \quad (7)$$

$$R\text{-}GO(h_{(VB)}^+) + H_2O \rightarrow 2({}^\bullet OH) \quad (8)$$

$${}^\bullet OH + BB3 \rightarrow \text{intermediate products} \quad (9)$$

3.4. Kinetic study of BB3 degradation

To determine the reaction rate and rate constants, kinetic studies were carried out. For this purpose, evaluation of the time effect on the BB3 degradation efficiency of the synthesized photocatalyst is crucial. The following mathematical formula represents the linear form of the pseudo-first-order model;[60]

$$\ln\left(\frac{C_0}{C_t}\right) = K_1 t \quad (10)$$

Based on the photocatalytic experiment results, the slope of the straight-line plot from the linear relationship between

irradiation time (t) and ($\ln C_0/C_t$) for dye degradation was determined for different samples used. Here, k_1 represents the apparent rate constant, C_0 is the initial dye concentration at $t = 0$ min, and C_t is the concentration at a given time. Moreover, the non-linear form of pseudo-first-order was also used to investigate the time-dependent behavior of all photocatalysts toward BB3 dye removal.[61]

$$q_t = q_e(1 - e^{(-K_1 t)}) \qquad (11)$$

The adsorption kinetics were analyzed using the pseudo-first-order model, where q_e represents the equilibrium adsorption capacity (mg g^{-1}) and q_t denotes the adsorption capacity at time t (min). The rate constant k_1 was determined from the slope of the non-linear regression fit of q_t versus time. As evidenced in Fig. 8(a and b), all photocatalysts exhibited degradation profiles that closely followed pseudo-first-order kinetics, with excellent correlation coefficients ($R^2 > 0.9$) confirming the validity of the model. Comparative analysis revealed the superior performance of Cu@R-GO, which demonstrated a rate constant 1.0625 fold higher than Cu@GO, 735.06 times greater activity than pristine GO, and 190.47 times enhanced performance *versus* RGO. These quantitative comparisons, summarized in Table 1, unequivocally demonstrate the remarkable catalytic enhancement achieved through copper modification of reduced graphene oxide. The kinetic parameters and corresponding correlation coefficients were directly extracted from the non-linear fitting of the experimental data presented in Fig. 8(a and b).

3.5. Thermodynamics study

To assess the thermodynamic parameters from the temperature-dependent photocatalytic degradation data for BB3, using Cu@GO and Cu@R-GO, the Eyring and Arrhenius's equations were used for analysis. The effect of temperature on the apparent rate constant (k_1) is explained by using the Arrhenius equation, as shown in eqn (12).[62]

$$\ln k_1 = \ln A - \left[\frac{E_A}{RT}\right] \qquad (12)$$

Table 1 Summary of the kinetics parameters determined from the linear and nonlinear pseudo-first-order models

Catalyst	Linear pseudo 1st-order		Non-linear pseudo 1st-order	
	Parameters	Values	Parameters	Values
GO	K_1 (min^{-1})	0.00458	Calculated q_e (mg g^{-1})	12.81
	R^2	0.933	K_1 (min^{-1})	2.31×10^{-5}
			R^2	0.933
R-GO	K_1 (min^{-1})	0.00616	Calculated q_e (mg g^{-1})	42.02
	R^2	0.980	K_1 (min^{-1})	8.92×10^{-5}
			R^2	0.98
Cu@GO	K_1 (min^{-1})	0.0130	Calculated q_e (mg g^{-1})	72.54
	R^2	0.942	K_1 (min^{-1})	0.016
			R^2	0.963
Cu@R-GO	K_1 (min^{-1})	0.0154	Calculated q_e (mg g^{-1})	76.93
	R^2	0.965	K_1 (min^{-1})	0.017
			R^2	0.98

Here, k_1 (min^{-1}) is the rate constant, R (J mol^{-1} K^{-1}) is the gas constant, A is the pre-exponential factor, and T (K) is the temperature. According to the Arrhenius equation, an inverse relationship exists between the parameters $\ln(k_1)$ and of $1/T$ (Fig. 9). As with an increase in temperature, the values of $1/T$ decline, and as a result, $\ln(k_1)$ values increase in the Arrhenius plot.[63] This suggests that the degradation rate increases at higher temperatures. The Arrhenius plots further confirm the pseudo-first-order kinetics by demonstrating a linear relationship between $\ln(k_1)$ and temperature. The activation energy (E_A) for the photocatalytic degradation of BB3 was determined to be 23.56 kJ mol^{-1} for Cu@GO and 25.30 kJ mol^{-1} for Cu@R-GO (Table 2). Also, as mentioned in eqn (13), the Eyring equation was employed to further explore the relationship between the apparent rate constant and temperature.[64]

$$\ln \frac{k_1}{T} = \ln \frac{k_B}{h} + \frac{\Delta S^*}{R} + \frac{\Delta H^*}{RT} \qquad (13)$$

The pseudo-first-order rate constant (k) was analyzed in relation to fundamental physical constants – Boltzmann's
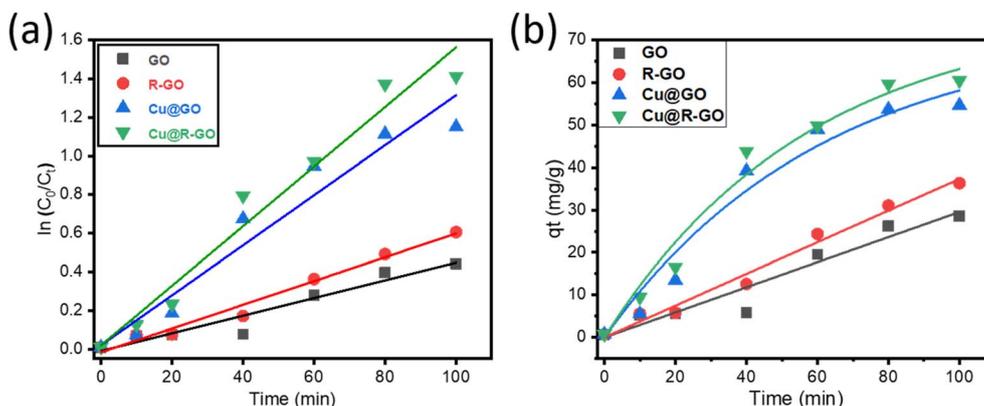
Fig. 8 Representative degradation plots of pseudo-first-order kinetics (a) linear and (b) non-linear, for GO, R-GO, Cu@GO, and Cu@R-GO.
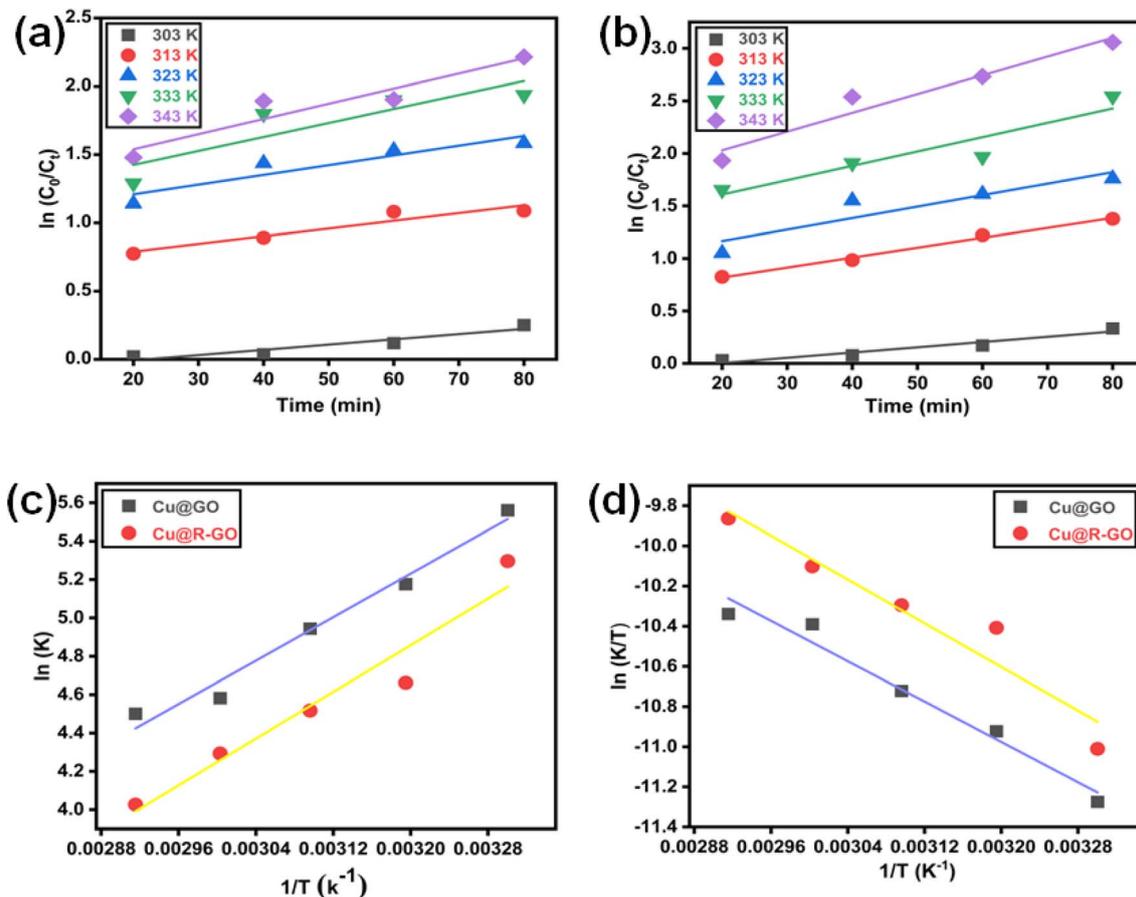
Fig. 9 Linear graphs illustrating the (a) pseudo-first-order kinetics graph of Cu@GO at different temperatures, (b) pseudo-first-order kinetics plot of Cu@R-GO at different temperatures, (c) Arrhenius plot for Cu@GO and Cu@R-GO, and (d) Eyring plot for Cu@GO and Cu@R-GO.

constant (k_B, J K^{-1}) and Planck's constant (h, J s) – to determine the thermodynamic parameters governing the degradation process. The activation entropy (ΔS) was calculated as 458.61 J mol^{-1} K^{-1} for Cu@GO and 459.95 J mol^{-1} K^{-1} for Cu@R-GO, while the activation enthalpy (ΔH) values were 20.89 kJ mol^{-1} and 22.62 kJ mol^{-1}, respectively. These results demonstrate that the photocatalytic degradation of Basic Blue 3 (BB3) at the catalyst–liquid interface is an endothermic process characterized by decreasing entropy during the reaction. The

temperature-dependent behavior, as shown in the Eyring plot in Fig. 9, reveals a linear correlation between ln(k/T) and $1/T$, confirming the validity of the Eyring equation for this system. The positive slope indicates enhanced degradation rates at elevated temperatures, consistent with the endothermic nature of the process. The thermodynamic parameters, including activation energy (E_a), entropy of activation (ΔS), and enthalpy of activation (ΔH), are systematically presented in Table 2.

Table 2 Important thermodynamic parameters determined using the Arrhenius and Eyring equations

Catalyst	E_a (kJ mol^{-1})	ΔH (kJ mol^{-1})	ΔS (J mol^{-1})	ΔG (kJ mol^{-1})	R^2 Arrhenius equation	R^2 Eyring equation
Cu@GO	23.56	20.89	458.61	−118.07 −122.66 −127.24 −131.83 −136.42	0.977	0.97
Cu@R-GO	25.30	22.62	449.95	−113.71 −118.21 −122.71 −127.21 −131.71	0.941	0.93

3.6. Comparative investigation on the dye removal efficiency of the synthesized materials with previous studies

To gain a deeper understanding of this study, a comparative analysis is provided to evaluate the performance of the synthesized catalysts with those reported previously against the dye removal efficiency. Table 3 highlights their superior performance, influenced by many factors such as catalyst type, dosage, dye concentration, contact time, pH, and temperature.

Table 3 Some comparative analysis on the dye removal efficiency of the synthesized materials with previous reports

| Materials	Dyes	Experimental conditions	Dyes concentration	% Removal	Reference
GO	MB	Catalyst dose: 0.01 g Time: 60 min, pH = 6 Sol = 20 mL, T = 30 °C	20 mg L^{-1}	22.8	65
GO-Fe$_3$O$_4$	RB	Catalyst dose: 0.01 g Time: 60 min, pH = 6 Sol = 20 mL, T = 30 °C	10 mg L^{-1}	70	66
Ni/GO-CNT	RhB	Catalyst dose: 0.025 g Time: 120 min, pH = 6 Sol = 250 mL, T = 25 °C, UV/H$_2$O$_2$ assisted	5 mg L^{-1}	73.6	67
ZnCr$_2$O$_4$-rGO	MB	Catalyst dose: 0.01 g Time: 70 min, pH = 8 Sol = 50 mL, T = 25 °C, UV/H$_2$O$_2$ assisted	10 mg L^{-1}	95.7	68
Fe$_3$O$_4$/rGO	MO	Catalyst dose: 0.25 g Time: 35 min, pH = 2.9 Sol = 100 mL, T = 50 °C, UV/H$_2$O$_2$ assisted	50 mg L^{-1}	99.8	69
rGO	NB	Catalyst dose: 0.01 g Time: 40 min, pH = 5 Sol: 20 mL, T = 30 °C	20 mg L^{-1}	92	70
CuO–SiO$_2$/PVA	NB	Catalyst dose: 0.01 g Time: 40 min, pH = 9 Sol: 100 mL, T = 30 °C	30 mg L^{-1}	58	71
g-C$_3$N$_4$/ZnCo$_2$O$_4$	CR	Catalyst dose: 0.01 g Time: 40 min, pH = 6 Sol: 100 mL, T = 30 °C	10 mg L^{-1}	99	72
Ag/rGO	NB	Catalyst dose: 0.01 g Time: 60 min, pH = 6 Sol: 100 mL, T = 30 °C	20 mg L^{-1}	92	10
Cu$_2$O/rGO	MB	Catalyst dose: 0.01 g Time: 100 min, pH = 9 Sol: 100 mL, T = 30 °C	50 mg L^{-1}	76	73
Ag@RGO/g-C$_3$N$_4$	AM	Catalyst dose: 0.01 g Time: 60 min, pH = 3 Sol: 100 mL, T = 30 °C	40 mg L^{-1}	77	74
CuWO$_4$	NB	Catalyst dose: 0.01 g Time: 100 min, pH = 11 Sol: 100 mL, T = 30 °C	10 mg L^{-1}	83	75
CNT/MgO/CuFe$_2$O$_4$	MVD	Catalyst dose: 0.01 g Time: 60 min, pH = 6 Sol: 100 mL, T = 30 °C	20 mg L^{-1}	99	12
GO	BB3	Catalyst dose: 0.01 g Time: 80 min, pH = 7 Sol: 100 mL, T = 30 °C	80 mg L^{-1}	35.2	This work
Cu@GO	BB3	Catalyst dose: 0.01 g Time: 80 min, pH = 7 Sol: 100 mL, T = 30 °C	80 mg L^{-1}	68.8	This work
R-GO	BB3	Catalyst dose: 0.01 g Time: 80 min, pH = 7 Sol: 100 mL, T = 30 °C	80 mg L^{-1}	41.4	This work
Cu@R-GO	BB3	Catalyst dose: 0.01 g Time: 80 min, pH = 7 Sol: 100 mL, T = 30 °C	80 mg L^{-1}	75.5	This work
Cu@R-GO	BB3	Catalyst dose: 0.01 g Time: 80 s min, pH = 7 Sol: 100 mL, T = 30 °C, UV/H$_2$O$_2$ assisted (9 m. mole)	80 mg L^{-1}	99.53	This work
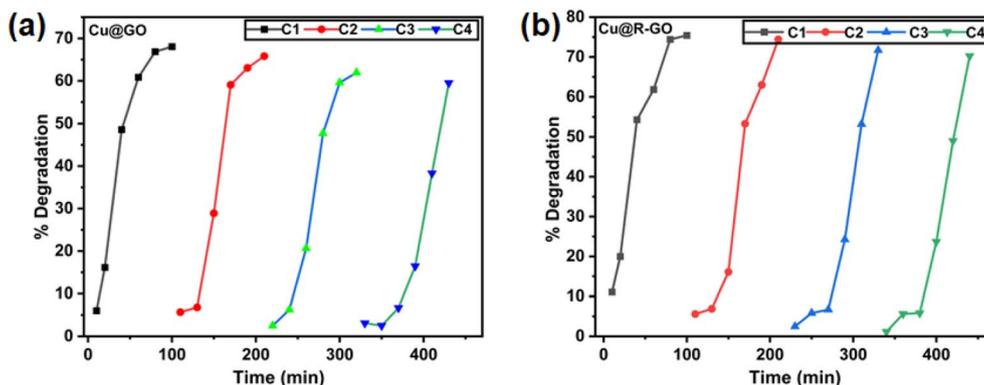
Fig. 10 Reusability of (a) Cu@GO and (b) Cu@R-GO for the BB3 dye degradation.

Dye molecules interact with the catalyst surface through different bonding forces, including hydrogen bonding, van der Waals dispersion forces, and electrostatic interaction, establishing equilibrium for effective dye removal. The chemical composition, surface texture, and morphology significantly impact the photocatalytic efficiency of the synthesized materials. Moreover, structural modifications from graphite to GO, R-GO, and Cu@GO, and Cu@R-GO enhance photocatalytic as well as adsorptive properties by altering the surface characteristics and bandgap energies. These enhancements are attained through cost-effective and scalable modification techniques, making Cu@R-GO a promising material for wastewater treatment.

3.7. Reusability of Cu@GO and Cu@R-GO

The capability of the catalysts is vital in determining their practical efficiency and environmental sustainability for applications such as wastewater purification, air pollution control, and the degradation of organic pollutants, especially dyes. In this study, we evaluated the reusability of the Cu@GO and Cu@R-GO photocatalysts by testing whether they retain their catalytic activity over multiple recycles. The durability of Cu@GO and Cu@R-GO nanocomposites towards the degradation of Basic Blue 3 (BB3) dye was tested over four consecutive cycles under the same experimental conditions, such as reaction time (80 minutes), concentration of dye (80 mg L^{-1}), pH (7), and catalyst dose (0.1 g), all at room temperature. After each cycle, the catalyst was recovered, washed several times with distilled water and ethanol, and dried at 70 °C for one hour. Notably, the catalysts showed excellent stability in the recycling experiments, with minimal loss in the removal efficiency. As illustrated in Fig. 10(a and b), the structure integrity and efficiency of the catalysts remained intact after four consecutive cycles. These results suggest that Cu@GO and Cu@R-GO are reliable and reusable materials for the photocatalytic degradation of BB3 dye under UV light.

3.8. Summary of advantages and limitations of the current study

This study focuses on comparing and evaluating the effectiveness of graphene oxide (GO), reduced graphene oxide (R-GO),

copper-decorated graphene oxide (Cu@GO) and copper-decorated reduced graphene oxide (Cu@R-GO) in removing hazardous pollutants, specifically Basic Blue 3 dye, from aqueous environments. This report provides a comprehensive analysis of their chemical composition, structure, and morphology. The results revealed that modifying GO and R-GO-based materials with copper (Cu) enhances their desired photocatalytic properties through a well-established, cost-effective *ex situ* approach. The method used here offers ease of preparation, reduced complexity, and lower costs compared to other techniques. The incorporation of copper nanoparticles into GO and R-GO to form Cu@GO and Cu@R-GO is expected to improve their photocatalytic performance significantly. Furthermore, the Cu@R-GO nanocomposite exhibits significant stability under the experimental conditions, making it a good material for wastewater treatment applications. The study primarily focused on the removal of Basic Blue 3 (BB3) dye using batch processes. However, real textile wastewater samples may contain a variety of extra pollutants and ions. Future research should explore the applicability of the synthesized materials for treating the actual wastewater samples from different textile industries. Additionally, developing effective strategies for the proper disposal or recycling of the catalysts after the dye removal process is important for sustainable wastewater treatment applications.

4 Conclusions

In this study, we successfully synthesized graphene oxide (GO), reduced graphene oxide (R-GO), copper-decorated (Cu@GO), and copper-decorated reduced graphene oxide (Cu@R-GO) using a cost-effective, *ex situ* method. The structural, thermal, texture, chemical, and morphological properties of the synthesized materials were analyzed using different spectroscopic techniques, confirming their successful fabrication. X-ray photoelectron spectroscopy (XPS) confirms the binding energies of Cu^0 and Cu$^+$ species, confirming the existence of metallic copper and/or Cu(I) in the composites. In Raman spectroscopy, the nanocomposites exhibited prominent D and G bands at almost 1350 cm^{-1} and 1580 cm^{-1}, respectively. The D band is related to structural defects and disordered sp^2 carbon, whereas

Paper

the G band corresponds to the in-plane vibrations of sp^2 carbon atoms. To check the adsorptive and photocatalytic efficiency of these materials for the removal of basic blue 3 (BB3) dye from wastewater, experiments were conducted under varying experimental conditions, including time, temperature, catalyst dose, dye concentration, pH, and the addition of hydrogen peroxide (H_2O_2). Among the synthesized nano-materials, Cu@R-GO and Cu@GO showed the highest photocatalytic performance, achieving a maximum removal rate of 99.9% and 97%, respectively, under optimal conditions: reaction time = 80 minutes, temperature = 60 °C, catalyst dose = 0.1 g, dye concentration = 80 mg L^{-1}, pH = 9, a UV-light source (35 W), and 9 mM of H_2O_2. To elucidate the underlying degradation mechanism and identify the dominant reactive oxygen species (ROS) involved in BB3 dye degradation under optimal conditions using Cu@R-GO, a series of scavenger experiments were conducted. The results indicate that hydroxyl radicals ($^\bullet$OH) and superoxide radicals ($^\bullet$O$_2^-$) are the primary active species, with photogenerated holes (h^+) also contributing significantly to the degradation process under the given experimental conditions. Kinetic studies revealed that BB3 degradation using GO, R-GO, Cu@R-GO, and Cu@GO followed both pseudo-first-order linear and non-linear kinetic models, with R^2 values exceeding 0.98. Thermodynamic analysis indicated that the degradation process was endothermic. The Cu@R-GO nanocomposite exhibited excellent stability, highlighting its potential as a promising candidate for wastewater treatment. The kinetic and thermodynamic results further suggest that the overall degradation mechanism is physicochemical in nature. This study contributes to the development of cost-effective and eco-friendly nanocomposites for photocatalytic applications.

Ethical statement

With the submission of this manuscript, we would like to undertake that this work is original research that has not been published before; that it is not under consideration for publication anywhere else; that its publication has been approved by all co-authors; and that our institute's representative is fully aware of its submission to Royal society of chemistry (RSC).

Author contributions

All authors have contributed to this study at different stages. Ubaid Ur Rahman, Abbas Khan, and Muhammad Humayun: study design, method design, analytical protocol design, writing, reviewing, and editing. Ubaid Ur Rahman, Muhammad Humayun, and Abbas Khan: experimental assistant, discussion during writing, and reviewing. Ubaid Ur Rahman and Abbas Khan: experimental assistant and data analysis. Ubaid Ur Rahman, Nasrullah Shah, Mohamed Bououdina, Abbas Khan, Amal Faleh Alanazi, Asadullah, and Muhammad Humayun: reviewing and editing. All authors read and approved the final version of this manuscript.

Conflicts of interest

No potential conflict of interest was reported by the author(s).

Data availability

The data used to support the findings of this study are available from the corresponding author upon request.

Detailed bandgap energy graphs, UV-visible absorption spectrum of photo-assisted removal of BB3 using GO, R-GO, Cu@GO and Cu@R-GO, and free radical trapping experiments for Cu@R-GO nanocomposite. See DOI: https://doi.org/10.1039/d5ra04107d.

Acknowledgements

References

1 S. Dave, J. Das, B. Varshney and V. Sharma, Dyes and pigments: Interventions and how safe and sustainable are colors of life, in *Trends and Contemporary Technologies for Photocatalytic Degradation of Dyes*, Springer, 2022, pp. 1–20.

2 A. Haleem, A. Shafiq, S.-Q. Chen and M. Nazar, A comprehensive review on adsorption, photocatalytic and chemical degradation of dyes and nitro-compounds over different kinds of porous and composite materials, *Molecules*, 2023, **28**(3), 1081.

3 W. Muhammad, S. Hussain, A. Khan, H. Khan, N. Khan, F. Wahab and S. Khan, Physicochemical Investigations of Magnetite Persulfate Ozone Hybrid System for the Removal of Tartrazine Dye from Aqueous Solution, *Ozone: Sci. Eng.*, 2025, **47**(1), 21–39.

4 M. Ismail, K. Akhtar, M. Khan, T. Kamal, M. A. Khan, A. M Asiri, J. Seo and S. B. Khan, Pollution, toxicity and carcinogenicity of organic dyes and their catalytic bio-remediation, *Curr. Pharm. Des.*, 2019, **25**(34), 3645–3663.

5 R. Saini and K. Choudhary, Toxic potential of azo dyes: A broader understanding, in *Hazardous Chemicals*, Elsevier, 2025, pp. 469–481.

6 M. D. Khan, A. Singh, M. Z. Khan, S. Tabraiz and J. Sheikh, Current perspectives, recent advancements, and efficiencies of various dye-containing wastewater treatment technologies, *J. Water Process Eng.*, 2023, **53**, 103579.

7 R. Sathya, M. V. Arasu, N. A. Al-Dhabi, P. Vijayaraghavan, S. Ilavenil and T. Rejiniemon, Towards sustainable wastewater treatment by biological methods–A challenges

and advantages of recent technologies, *Urban Clim.*, 2023, **47**, 101378.

8 W. Muhammad, S. Hussain, A. Khan, I. Khan, M. Bououdina and M. Humayun, Enabling highly efficient navy-blue dye degradation over the LaFeO3/Bg-C3N4/WO3 double z-scheme heterostructure, *J. Alloys Compd.*, 2024, **1007**, 176435.

9 X. Ren, Y. Wang, A. Liu, Z. Zhang, Q. Lv and B. Liu, Current progress and performance improvement of Pt/C catalysts for fuel cells, *J. Mater. Chem. A*, 2020, **8**(46), 24284–24306.

10 Natasha, A. Khan, U. U. Rahman, Sadaf, M. Yaseen, R. A. Abumousa, R. Khattak, N. Rehman, M. Bououdina and M. Humayun, Effective removal of nile blue dye from wastewater using silver-decorated reduced graphene oxide, *ACS Omega*, 2024, **9**(17), 19461–19480.

11 S. F. Ahmed, P. S. Kumar, B. Ahmed, T. Mehnaz, G. Shafiullah, X. Q. Duong, M. Mofijur, I. A. Badruddin and S. Kamangar, Carbon-based nanomaterials: characteristics, dimensions, advances and challenges in enhancing photocatalytic hydrogen production, *Int. J. Hydrogen Energy*, 2024, **52**, 424–442.

12 B. Barzegar, S. J. Peighambardoust, H. Aghdasinia and R. Foroutan, Multi-characteristic optimization and modeling analysis of Cu2+ removal from wastewater using activated coke/MnFe2O4 magnetic composite, *J. Water Process Eng.*, 2023, **53**, 103803.

13 M. Iordache, A. Oubraham, I.-S. Sorlei, F. A. Lungu, C. Capris, T. Popescu and A. Marinoiu, Noble metals functionalized on graphene oxide obtained by different methods—new catalytic materials, *Nanomaterials*, 2023, **13**(4), 783.

14 M. Heshami, Z. Tavangar and B. Taheri, Adsorption of gold and silver glycinate on graphene and graphene oxide surface: A DFT study, *Appl. Surf. Sci.*, 2023, **619**, 156676.

15 A. Khan, S. Iqbal, S. Batool, S. Musaddiq and F. Iqbal, Understanding Photocatalytic Mechanism Through Spectroscopy Techniques, in *Graphene-Based Photocatalysts for Hydrogen Production and Environmental Remediation*, Springer, 2024, pp. 115–145.

16 L. Fritea, F. Banica, T. O. Costea, L. Moldovan, L. Dobjanschi, M. Muresan and S. Cavalu, Metal nanoparticles and carbon-based nanomaterials for improved performances of electrochemical (Bio) sensors with biomedical applications, *Materials*, 2021, **14**(21), 6319.

17 S. Agnihotri and N. K. Dhiman, Development of nano-antimicrobial biomaterials for biomedical applications, *Advances in Biomaterials for Biomedical Applications*, 2017, pp. 479–545.

18 M. T. M. H. Hamad and M. E. El-Sesy, Adsorptive removal of levofloxacin and antibiotic resistance genes from hospital wastewater by nano-zero-valent iron and nano-copper using kinetic studies and response surface methodology, *Bioresour. Bioprocess.*, 2023, **10**(1), 1.

19 S. Gunes-Durak, S. Acarer-Arat, M. Tufekci, İ. Pir, Z. Üstkaya, N. Öz and N. e. Tüfekci, Mechanical Enhancement and Water Treatment Efficiency of Nanocomposite PES Membranes: A Study on Akçaay Dam Water Filtration Application, *ACS Omega*, 2024, **9**(29), 31556–31568.

20 U. S. Meda, V. G. Soundarya, H. Madhu and N. Bhat, Nano-engineered textiles: development and applications, *Mater. Sci. Eng., B*, 2023, **296**, 116636.

21 K. Thakur and B. Kandasubramanian, Graphene and graphene oxide-based composites for removal of organic pollutants: a review, *J. Chem. Eng. Data*, 2019, **64**(3), 833–867.

22 K. Obaideen, N. Shehata, E. T. Sayed, M. A. Abdelkareem, M. S. Mahmoud and A. Olabi, The role of wastewater treatment in achieving sustainable development goals (SDGs) and sustainability guideline, *Energy Nexus*, 2022, **7**, 100112.

23 A. Punia and S. K. Singh, Contamination of water resources in the mining region, in *Contamination of Water*, Elsevier, 2021, pp. 3–17.

24 R. I. Alsantali, Q. A. Raja, A. Y. Alzahrani, A. Sadiq, N. Naeem, E. U. Mughal, M. M. Al-Rooqi, N. El Guesmi, Z. Moussa and S. A. Ahmed, Miscellaneous azo dyes: a comprehensive review on recent advancements in biological and industrial applications, *Dyes Pigm.*, 2022, **199**, 110050.

25 N. Hemashenpagam and S. Selvajeyanthi, Textile dyes and their effect on human beings, in *Nanohybrid Materials for Treatment of Textiles Dyes*, Springer, 2023, pp. 41–60.

26 K. O. Badmus, J. O. Tijani, E. Massima and L. Petrik, Treatment of persistent organic pollutants in wastewater using hydrodynamic cavitation in synergy with advanced oxidation process, *Environ. Sci. Pollut. Res.*, 2018, **25**, 7299–7314.

27 R. Rashid, I. Shafiq, P. Akhter, M. J. Iqbal and M. Hussain, A state-of-the-art review on wastewater treatment techniques: the effectiveness of adsorption method, *Environ. Sci. Pollut. Res.*, 2021, **28**, 9050–9066.

28 A. Dawood, M. A. Khan, S. Ullah, I. Ali, S. Saghir, Z. Ullah, A. Ayub, Z. Jabeen, J. Ahmad and M. S. Khan, High-performance nano assemblies for heavy-metal filtration from wastewater, *Nano-Struct. Nano-Objects*, 2024, **39**, 101209.

29 M. Zahran, Carbohydrate polymer-supported metal and metal oxide nanoparticles for constructing electrochemical sensors, *Mater. Adv.*, 2024, **5**(1), 68–82.

30 I. Fatimah, G. Fadillah, I. Yanti and R.-a. Doong, Clay-supported metal oxide nanoparticles in catalytic advanced oxidation processes: a review, *Nanomaterials*, 2022, **12**(5), 825.

31 A. M. Abu-Dief and W. Mohamed, Development of nanomaterials as photo catalysts for environmental applications, *Curr. Catal.*, 2020, **9**(2), 128–137.

32 C. Imparato, A. Bifulco, B. Silvestri and G. Vitiello, Recent advances in endocrine disrupting compounds degradation through metal oxide-based nanomaterials, *Catalysts*, 2022, **12**(3), 289.

33 B. A. Aragaw and A. Dagnaw, Copper/reduced graphene oxide nanocomposite for high performance photocatalytic methylene blue dye degradation, *Ethiop. J. Sci. Technol.*, 2019, **12**(2), 125–137.

34 M. Ikram, S. Ali, M. Aqeel, A. Ul-Hamid, M. Imran, J. Haider, A. Haider, A. Shahbaz and S. Ali, Reduced graphene oxide nanosheets doped by Cu with highly efficient visible light photocatalytic behavior, *J. Alloys Compd.*, 2020, **837**, 155588.

35 S. Sagadevan, J. A. Lett, G. K. Weldegebrieal, S. Garg, W.-C. Oh, N. A. Hamizi and M. R. Johan, Enhanced photocatalytic activity of rGO-CuO nanocomposites for the degradation of organic pollutants, *Catalysts*, 2021, **11**(8), 1008.

36 S. Kumaran, P. Buvaneswari, K. Shree and V. Rajmohan, Fabrication of rGO-modified ternary metal chalcogenide hybrid nanocomposite (rGO/Cu2MnSnS4) for high-performance supercapacitors, *Diamond Relat. Mater.*, 2024, **148**, 111384.

37 F. J. Alguacil, M. Alonso and J. I. Robla, Removal of Hazardous Organic Dyes from Liquid Wastes Using Advanced Nanomaterials, *Int. J. Mol. Sci.*, 2024, **25**(17), 9671.

38 A. Jafari, M. Majdoub, D. Sengottuvelu, M. G. Ucak-Astarlioglu, A. Al-Ostaz and S. Nouranian, Tribological Properties of Synthetic and Biosourced Lubricants Enhanced by Graphene and Its Derivatives: A Review, *ACS Omega*, 2024, **9**(52), 50868–50893.

39 I. Sengupta, S. S. S. Kumar, S. K. Pal and S. Chakraborty, Investigating the effect of graphite pretreatment and contribution of the oxidizer in the synthesis of graphite oxide by hummers approach, *Fullerenes, Nanotubes Carbon Nanostruct.*, 2022, **30**(6), 626–637.

40 F. Sun, From Graphene Oxide to Reduced Graphene Oxide, in *Synthesis and Device Applications of Graphene Derivatives and Quantum Dots*, Springer, 2024, pp. 31–48.

41 D. Akyüz, rGO-TiO2-CdO-ZnO-Ag photocatalyst for enhancing photocatalytic degradation of methylene blue, *Opt. Mater.*, 2021, **116**, 111090.

42 U. U. Rahman, M. Humayun, A. Khan, S. Farooq, M. Sadiq, M. Bououdina and N. Shah, Thermo-chemical modification of cellulose for the adsorptive removal of titan yellow from wastewater, *Molecules*, 2023, **28**(9), 3955.

43 A. Sahai, N. Goswami, S. Kaushik and S. Tripathi, Cu/Cu2O/CuO nanoparticles: Novel synthesis by exploding wire technique and extensive characterization, *Appl. Surf. Sci.*, 2016, **390**, 974–983.

44 K. Mikami, Y. Kido, Y. Akaishi, A. Quitain and T. Kida, Synthesis of Cu2O/CuO nanocrystals and their application to H2S sensing, *Sensors*, 2019, **19**(1), 211.

45 A. Asadullah, A. Khan, U. Ur Rahman, M. Humayun, A. Akbar, A. Faleh Alanazi and M. Bououdina, Green Synthesis of Zinc Oxide-Graphene Oxide Composite via Ex Situ and In Situ Methods for the Photoassisted Removal of Congo Red Dye: A Comparative Study, *ACS Omega*, 2025, **25**(10), 27112–27126.

46 A. C. Ferrari and D. M. Basko, Raman spectroscopy as a versatile tool for studying the properties of graphene, *Nat. Nanotechnol.*, 2013, **8**(4), 235–246.

47 F. Li, A. Gong, L. Qiu, W. Zhang, J. Li and Z. Liu, Diglycolamide-grafted Fe3O4/polydopamine nanomaterial as a novel magnetic adsorbent for preconcentration of rare earth elements in water samples prior to inductively coupled plasma optical emission spectrometry determination, *Chem. Eng. J.*, 2019, **361**, 1098–1109.

48 T. Tene, M. Guevara, F. Benalcázar Palacios, T. P. Morocho Barrionuevo, C. Vacacela Gomez and S. Bellucci, Optical properties of graphene oxide, *Front. Chem.*, 2023, **11**, 1214072.

49 T. Tene, Y. Jiménez-Gaona, D. K. Campoverde-Santos, Y. Cevallos, M. La Pietra, C. Vacacela Gomez, A. Scarcello, S. Straface, L. S. Caputi and S. Bellucci, Tunable optical and semiconducting properties of eco-friendly-prepared reduced graphene oxide, *Front. Chem.*, 2023, **11**, 1267199.

50 G. A. Sundaram, S. Kumaravelu, W.-L. Tseng, P. V. Pham, A. S. K. Kumar and V. Parimelazhagan, Fine-tuned graphene oxide nanocomposite: harnessing copper (II)–imidazole complex for enhanced biological responses and balanced photocatalytic functionality, *Materials*, 2024, **17**(4), 892.

51 A. Kumawat; N. S. Leel, Enhancement of Optical and Surface Electronic Properties in Rgo-Cuo Nanocomposites for Improved Photocatalytic Activities.

52 C. Pei, A. A. Aryee, K. Zhu, R. Wang and R. Han, Adsorption and catalytic degradation of Light green SF by magnetic PEI-modified carbon nanotubes composites, *Sep. Purif. Technol.*, 2025, **355**, 129625.

53 W. Muhammad, S. Hussain, A. Khan, H. Khan, N. Khan, S. U. Khan, S. Ali, M. Bououdina and M. Humayun, Novel magnetite/persulphate/ozone hybrid system for catalytic degradation/ozonation of sunset yellow dye from wastewater, *Nanocomposites*, 2024, **10**(1), 109–124.

54 S. Sağlam, F. N. Türk and H. Arslanoğlu, Use and applications of metal-organic frameworks (MOF) in dye adsorption, *J. Environ. Chem. Eng.*, 2023, 110568.

55 M.-C. Stanciu and C.-A. Teacă, Natural Polysaccharide-Based Hydrogels Used for Dye Removal, *Gels*, 2024, **10**(4), 243.

56 G. Martemucci, C. Costagliola, M. Mariano, L. D'andrea, P. Napolitano and A. G. D'Alessandro, Free radical properties, source and targets, antioxidant consumption and health, *Oxygen*, 2022, **2**(2), 48–78.

57 H. Liang, J. Zhao, A. Brouzgou, A. Wang, S. Jing, P. Kannan, F. Chen and P. Tsiakaras, Efficient photocatalytic H2O2 production and photodegradation of RhB over K-doped g-C3N4/ZnO S-scheme heterojunction, *J. Colloid Interface Sci.*, 2025, **677**, 1120–1133.

58 G. Y. Abate, A. N. Alene, A. T. Habte and Y. A. Addis, Adsorptive removal of basic green dye from aqueous solution using humic acid modified magnetite nanoparticles: kinetics, equilibrium and thermodynamic studies, *J. Polym. Environ.*, 2021, **29**, 967–984.

59 H. Khan, Graphene based semiconductor oxide photocatalysts for photocatalytic hydrogen (H2) production, a review, *Int. J. Hydrogen Energy*, 2024, **84**, 356–371.

60 N. S. Ali, H. N. Harharah, I. K. Salih, N. M. Cata Saady, S. Zendehboudi and T. M. Albayati, Applying MCM-48 mesoporous material, equilibrium, isotherm, and mechanism for the effective adsorption of 4-nitroaniline from wastewater, *Sci. Rep.*, 2023, **13**(1), 9837.

61 J. Tsaviv, I. Eneji, R. Shato'Ato, I. Ahemen, P. Jubu and Y. Yusof, Photodegradation, kinetics and non-linear error functions of methylene blue dye using $SrZrO_3$ perovskite photocatalyst, *Heliyon*, 2024, **10**(14), e34517.

62 M. Shaban, R. Saad and A. M. El Sayed, Influence of chromium and lanthanum incorporation on the optical properties, catalytic activity, and stability of IrOx nanostructured films for hydrogen generation, *Int. J. Hydrogen Energy*, 2023, **48**(38), 14255–14270.

63 W. Muhammad, A. Khan, S. Hussain, H. Khan, R. A. Abumousa, M. Bououdina, I. Khan, S. Iqbal and M. Humayun, Enhanced light absorption and charge carrier's separation in g-C3N4-based double Z-scheme heterostructure photocatalyst for efficient degradation of navy-blue dye, *Green Chem. Lett. Rev.*, 2024, **17**(1), 2381591.

64 G. Gupta, D. Choudhury, R. Maurya, S. Sharma and M. Neergat, Investigation of Hydrogen Oxidation/Evolution Reactions Based on Charge-Transfer Coefficients Derived from Butler–Volmer and Eyring Analyses, *J. Phys. Chem. C*, 2023, **127**(49), 23566–23576.

65 F. Liu, S. Chung, G. Oh and T. S. Seo, Three-dimensional graphene oxide nanostructure for fast and efficient water-soluble dye removal, *ACS Appl. Mater. Interfaces*, 2012, **4**(2), 922–927.

66 S. Muthuvijayan, D. Banerjee, S. Chatterjee, T. Theivasanthi and S. C. Gopinath, Nitrogen-doped graphene and iron oxide nanoparticles for photocatalytic degradation, *J. Taiwan Inst. Chem. Eng.*, 2025, **168**, 105950.

67 C. Hu, A. T. Le, S. Y. Pung, L. Stevens, N. Neate, X. Hou, D. Grant and F. Xu, Efficient dye-removal via Ni-decorated graphene oxide-carbon nanotube nanocomposites, *Mater. Chem. Phys.*, 2021, **260**, 124117.

68 K. Tantubay, P. Das and M. Baskey, Hydrogen peroxide–assisted photocatalytic dye degradation over reduced graphene oxide integrated ZnCr2O4 nanoparticles, *Environ. Sci. Pollut. Res.*, 2022, **29**(12), 17309–17318.

69 H.-Y. Xu, Y. Wang, T.-N. Shi, X.-L. He and S.-Y. Qi, Process optimization on methyl orange discoloration in Fe3O4/ RGO-H2O2 Fenton-like system, *Water Sci. Technol.*, 2018, **77**(12), 2929–2939.

70 M. Ghalkhani, N. Zare, F. Karimi, C. Karaman, M. Alizadeh and Y. Vasseghian, Recent advances in Ponceau dyes monitoring as food colorant substances by electrochemical sensors and developed procedures for their removal from real samples, *Food Chem. Toxicol.*, 2022, **161**, 112830.

71 M. Yaseen, A. Khan, M. Humayun, S. Bibi, S. Farooq, M. Bououdina and S. Ahmad, Fabrication and characterization of CuO–SiO2/PVA polymer nanocomposite for effective wastewater treatment and prospective biological applications, *Green Chem. Lett. Rev.*, 2024, **17**(1), 2321251.

72 N. T. M. Huong, P. T. T. Hoai, K. TaeYoung and P. T. Huong, Exploring Cu-doped graphitic carbon nitride for treatment of dye pollutants in textile wastewater: Benefits and limitations, *Diamond Relat. Mater.*, 2024, **146**, 111160.

73 A. Muthukrishnaraj, S. A. Al-Zahrani, A. Al Otaibi, S. S. Kalaivani, A. Manikandan, N. Balasubramanian, A. L. Bilgrami, M. A. R. Ahamed, A. Khan and A. M. Asiri, Enhanced photocatalytic activity of Cu2O Cabbage/RGO nanocomposites under visible light irradiation, *Polymers*, 2021, **13**(11), 1712.

74 M. A. Hamza, S. A. Abd El-Rahman, A. N. El-Shazly, E. M. Hashem, R. T. Mohamed, E. M. El-Tanany and M. G. Elmahgary, Facile one-pot ultrasonic-assisted synthesis of novel Ag@ RGO/g-C3N4 ternary 0D@ 2D/2D nanocomposite with enhanced synergetic tandem adsorption-photocatalytic degradation of recalcitrant organic dyes: Kinetic and mechanistic insights, *Mater. Res. Bull.*, 2021, **142**, 111386.

75 T. Thiyagarajan, V. Deivasigamani, M. Raj, C. Joseph, T. Dheivasigamani, B. Palanivel, M. S. Hamdy and M. Shkir, Facile synthesis and characterization of WO3/ CuWO4 nanocomposites for the removal of toxic methylene blue dye, *Korean J. Chem. Eng.*, 2021, **38**(5), 952–965.